PALEOSEISMOLOGY OF UTAH, VOLUME 22

LATE HOLOCENE EARTHQUAKE HISTORY OF THE BRIGHAM CITY SEGMENT OF THE WASATCH FAULT ZONE AT THE HANSEN CANYON, KOTTER CANYON, AND PEARSONS CANYON TRENCH SITES, BOX ELDER COUNTY, UTAH

Christopher B. DuRoss, Stephen F. Personius, Anthony J. Crone, Greg N. McDonald, and Richard W. Briggs

SPECIAL STUDY 142
UTAH GEOLOGICAL SURVEY
a division of
UTAH DEPARTMENT OF NATURAL RESOURCES
2012

PALEOSEISMOLOGY OF UTAH, VOLUME 22

LATE HOLOCENE EARTHQUAKE HISTORY OF THE BRIGHAM CITY SEGMENT OF THE WASATCH FAULT ZONE AT THE HANSEN CANYON, KOTTER CANYON, AND PEARSONS CANYON TRENCH SITES, BOX ELDER COUNTY, UTAH

Christopher B. DuRoss[1], Stephen F. Personius[2], Anthony J. Crone[2], Greg N. McDonald[1], and Richard W. Briggs[2]

[1]Utah Geological Survey, Salt Lake City, Utah
[2]U.S. Geological Survey, Denver, Colorado

Cover photo: *Photographs of the Kotter Canyon (upper left), Hansen Canyon (upper right), and Pearsons Canyon (lower left) trench sites (May 2008). Lower-right photograph shows an exposure of the Wasatch fault (orange markers) at the Pearsons Canyon site (May 2008); grid spacing is 1 m.*

ISBN: 978-1-55791-861-1

SPECIAL STUDY 142
UTAH GEOLOGICAL SURVEY
a division of
UTAH DEPARTMENT OF NATURAL RESOURCES
2012

STATE OF UTAH
Gary R. Herbert, Governor

DEPARTMENT OF NATURAL RESOURCES
Michael Styler, Executive Director

UTAH GEOLOGICAL SURVEY
Richard G. Allis, Director

PUBLICATIONS
contact
Natural Resources Map & Bookstore
1594 W. North Temple
Salt Lake City, UT 84114
telephone: 801-537-3320
toll-free: 1-888-UTAH MAP
website: mapstore.utah.gov
email: geostore@utah.gov

UTAH GEOLOGICAL SURVEY
contact
1594 W. North Temple, Suite 3110
Salt Lake City, UT 84114
telephone: 801-537-3300
website: geology.utah.gov

Research supported by the U.S. Geological Survey (USGS), Department of the Interior, under USGS National Earthquake Hazards Reduction Program (NEHRP) award number 08HQGR0082. The views and conclusions contained in this document are those of the authors and should not be interpreted as necessarily representing the official policies, either expressed or implied, of the U.S. Government.

CONTENTS

FIGURES

TABLES

PLATES

FOREWORD

This Utah Geological Survey Special Study, *Late Holocene Earthquake History of the Brigham City Segment of the Wasatch Fault Zone at the Hansen Canyon, Kotter Canyon, and Pearsons Canyon trench sites, Box Elder County, Utah*, is the twenty-second report in the Paleoseismology of Utah series. This series makes the results of paleoseismic investigations in Utah available to geoscientists, engineers, planners, public officials, and the general public. These studies provide critical information regarding paleoearthquake parameters such as earthquake timing, recurrence, displacement, slip rate, fault geometry, and segmentation, which can be used to characterize potential seismic sources and evaluate the long-term seismic hazard of Utah's Quaternary faults.

This report presents new paleoseismic information for the Brigham City segment (BCS)—the northernmost of the five most active, central segments of the Wasatch fault zone (WFZ)—collected as part of a joint Utah Geological Survey (UGS) and U.S. Geological Survey (USGS) seismic-hazard evaluation. The BCS has a long elapsed time since its most recent surface-faulting earthquake (~2.1 kyr), which is over 1.5 times the segment's mean Holocene earthquake recurrence interval (~1.3 kyr). Thus, of the central WFZ segments, the BCS has the highest time-dependent probability of having a future surface-faulting earthquake. To better define the timing of the BCS's most recent surface-faulting earthquake, the UGS and USGS excavated trenches at three sites: two on the northern BCS at Hansen and Kotter Canyons, and one farther south near Pearsons Canyon. The Hansen and Kotter Canyon trenches showed that the most recent earthquake on the northern BCS occurred before 2 ka. At Pearsons Canyon, the most recent earthquake occurred at 1.2 ± 0.04 ka, which is consistent with field observations of scarps on the southern part of the segment having 1–2 m of surface offset on presumed late Holocene alluvial-fan surfaces. The 1.2-ka earthquake on the southern BCS likely represents the continuation of Weber-segment surface faulting across the Weber-Brigham City segment boundary at 1.1 ± 0.6 ka.

These data clarify the late Holocene surface-faulting history of the BCS, and importantly, confirm the long elapsed time since the most recent earthquake on most of the BCS. In addition, this study is the first to use paleoseismic (earthquake timing and displacement) data to document earthquake rupture across a WFZ segment boundary. Obtaining a complete Holocene paleoseismic record for the BCS is critical to understanding the segmentation of the northern WFZ, for refining probabilistic earthquake-hazard assessments, and improving earthquake-hazard evaluations for the region, all of which will ultimately help reduce Utah's earthquake-related risk.

William R. Lund, Editor
Paleoseismology of Utah Series

PALEOSEISMOLOGY OF UTAH, VOLUME 22

LATE HOLOCENE EARTHQUAKE HISTORY OF THE BRIGHAM CITY SEGMENT OF THE WASATCH FAULT ZONE AT THE HANSEN CANYON, KOTTER CANYON, AND PEARSONS CANYON TRENCH SITES, BOX ELDER COUNTY, UTAH

Christopher B. DuRoss, Stephen F. Personius, Anthony J. Crone, Greg N. McDonald, and Richard W. Briggs

ABSTRACT

Of the five central segments of the Wasatch fault zone (WFZ) having evidence of recurrent Holocene surface-faulting earthquakes, the Brigham City segment (BCS) has the longest elapsed time since its most recent surface-faulting event (~2.1 kyr) compared to its mean recurrence time between events (~1.3 kyr). Thus, the BCS has the highest time-dependent earthquake probability of the central WFZ. We excavated trenches at three sites—the Kotter Canyon and Hansen Canyon sites on the north-central BCS and Pearsons Canyon site on the southern BCS—to determine whether a surface-faulting earthquake younger than 2.1 ka occurred on the BCS. Paleoseismic data for Hansen Canyon and Kotter Canyon confirm that the youngest earthquake on the north-central BCS occurred before 2 ka, consistent with previous north-central BCS investigations at Bowden Canyon and Box Elder Canyon. At Hansen Canyon, the most recent earthquake is constrained to 2.1–4.2 ka and had 0.6–2.5 m of vertical displacement. At Kotter Canyon, we found evidence for two events at 2.5 ± 0.3 ka and 3.5 ± 0.3 ka, with an average displacement per event of 1.9–2.3 m. Paleoseismic data from Pearsons Canyon, on the previously unstudied southern BCS, indicate that a post-2 ka earthquake ruptured this part of the segment. The Pearsons Canyon earthquake occurred at 1.2 ± 0.04 ka and had 0.1–0.8 m of vertical displacement, consistent with our observation of continuous, youthful scarps on the southern 9 km of the BCS having 1–2 m of late Holocene(?) surface offset. The 1.2-ka earthquake on the southern BCS likely represents rupture across the Weber–Brigham City segment boundary from the penultimate Weber-segment earthquake at about 1.1 ka. The Pearsons Canyon data result in a revised length of the BCS that has not ruptured since 2 ka (with time-dependent probability implications), and provide compelling evidence of at least one segment-boundary failure and multi-segment rupture on the central WFZ. Our paleoseismic investigations of the BCS clarify the timing, displacement, and extent of late Holocene earthquakes on the segment, and importantly, confirm the long elapsed time since the most recent earthquake on most of the BCS.

INTRODUCTION

The Wasatch fault zone (WFZ) presents a significant earthquake hazard to Utah's heavily urbanized Wasatch Front. No historical large-magnitude earthquakes have occurred on the fault, but prominent fault scarps and the results of paleoseismic trench investigations completed in the past three decades (see compilation in Lund, 2005) show that it is capable of generating large-magnitude, surface-faulting earthquakes and that much of the fault has been active during the Holocene. These paleoseismic data are critical to characterizing earthquake timing, frequency, and size; to improving models of fault segmentation (e.g., Machette and others, 1992) and probabilistic ground shaking (e.g., Petersen and others, 2008); and to predicting, preparing for, and reducing Utah's future earthquake losses.

Recent fault-trench investigations on the WFZ—including those of McCalpin (2002), McCalpin and Forman (2002), Nelson and others (2006), Machette and others (2007), DuRoss and others (2008, 2009), and Olig and others (2011)—have improved our understanding of surface-faulting earthquakes on the five central and most densely populated fault segments. However, important questions remain regarding the most recent earthquake on the Brigham City segment (BCS), which—taking into account its Holocene earthquake history—has the highest time-dependent likelihood of a future surface-faulting earthquake of all WFZ segments (McCalpin and Nishenko, 1996; McCalpin and Forman, 2002). In this study, we present the results of a joint Utah Geological Survey (UGS) and U.S. Geological Survey (USGS) paleoseismic study of the BCS, focusing on the timing and displacement of the most recent earthquakes at three trench sites, and their implications for the segmentation of the northern WFZ.

Wasatch Fault Zone

The WFZ (figure 1) is the principal structural boundary between the actively extending Basin and Range Province and the relatively more stable Middle Rocky Mountain and

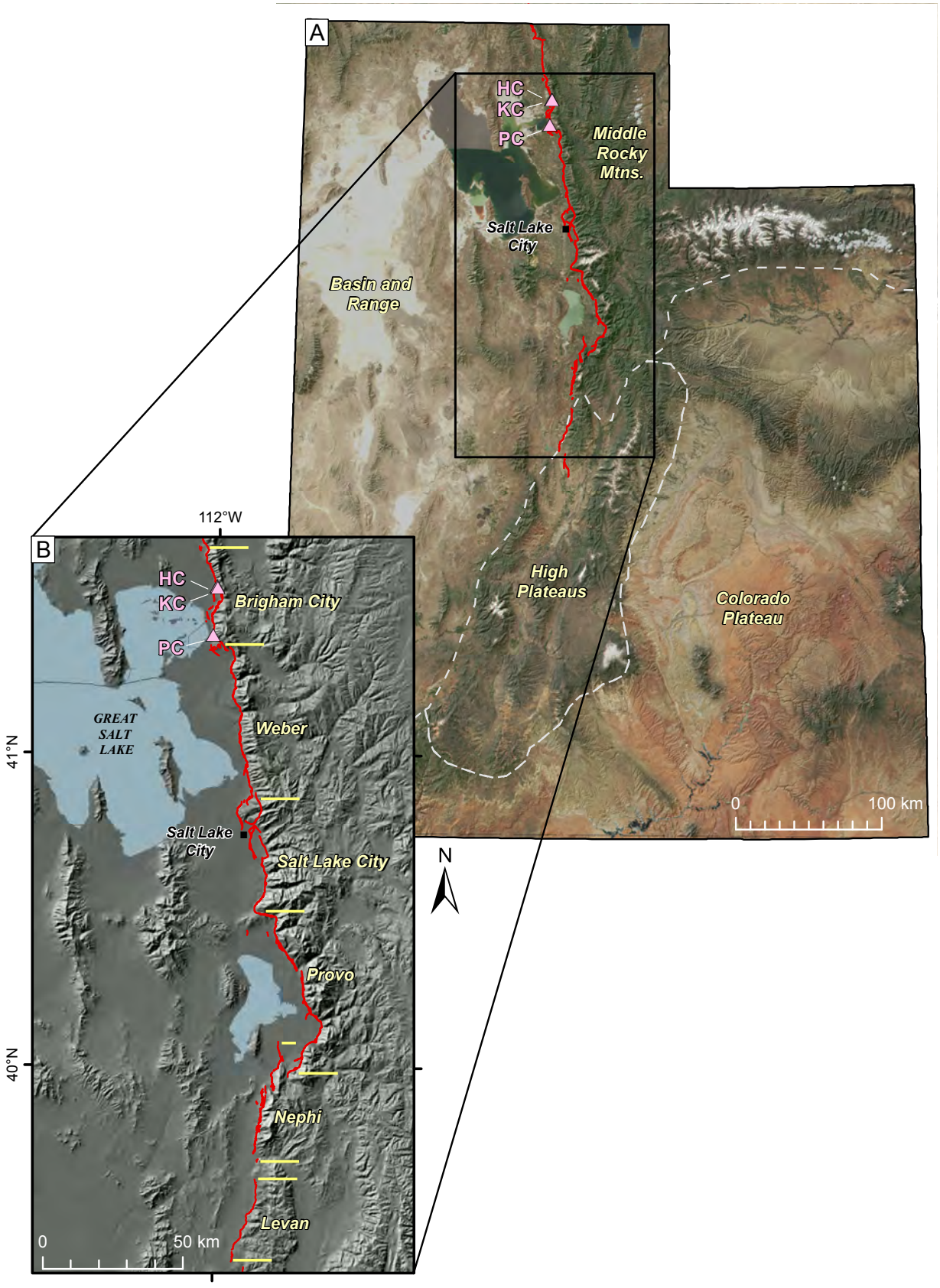

Figure 1. *(A) Physiographic provinces of Utah (gray dashed lines), showing the Wasatch fault (red) and Hansen Canyon (HC), Kotter Canyon (KC), and Pearsons Canyon (PC) trench sites. Base map: true-color satellite image from National Aeronautics & Space Administration (NASA, 2006; taken May 31, 2001) overlain on a 90-m digital elevation model (DEM) (Utah Automated Geographic Reference Center [UAGRC], 2012). (B) Central segments of the Wasatch fault zone. Horizontal yellow lines indicate segment boundaries. Base map: 90-m DEM (UAGRC, 2012).*

Colorado Plateau provinces in north-central Utah. The fault accommodates about 50 percent of the east-west extension across the eastern 200 km of the Basin and Range Province (easternmost Nevada to central Utah; Chang and others, 2006), and releases strain in large-magnitude (about M 6.5–7.5) surface-faulting earthquakes along seismogenic fault segments that are thought to generally rupture independently. The WFZ has been divided into 10 segments based on structural, geomorphic, geological, geophysical, and seismological data and characteristics (Machette and others, 1992). Of these, six segments (Brigham City to Levan; figure 1) have evidence for Holocene surface-faulting earthquakes (Swan and others, 1980; Schwartz and Coppersmith, 1984; Machette and others, 1992; Lund, 2005). Variations in the Holocene rupture history of the fault, and the geometry of late Quaternary fault traces are the primary evidence used to define the segment boundaries separating these six segments.

Five central segments of the WFZ (Brigham City to Nephi; figure 1) show evidence for recurrent Holocene earthquakes. Since the mid-Holocene (~6.5 ka), surface-faulting earthquakes have occurred on average every 1300–2500 yr per segment or every 350–400 yr collectively (Machette and others, 1992; McCalpin and Nishenko, 1996; Lund, 2005). Individual segments are 36–59 km long (straight-line distance; Machette and others, 1992; Black and others, 2003); measurements of vertical displacement from trench sites indicate that the mean per-event displacement ranges from about 1.7 m (Brigham City segment) to 2.9 m (Provo segment), or 2.2 ± 1.0 (1σ) for the central segments as a whole (DuRoss, 2008). The Holocene vertical slip rate on these segments is about 0.5–2.2 mm/yr based on paleoseismic and geomorphic rates compiled by Machette and others (1992; 0.5–1.5 mm/yr), Friedrich and others (2003; 1.2–2.2 mm/yr), and Lund (2005; average per segment of 1.1–1.4 mm/yr). The contemporary geodetic rate of horizontal extension is 1.2–2.0 mm/yr, assuming spatially homogeneous strain in a 65-km-wide zone across the fault (Chang and others, 2006). Recent advances in understanding the earthquake history of the central WFZ include refinements of early Holocene and latest Pleistocene paleoseismic records (McCalpin, 2002; McCalpin and Forman, 2002; DuRoss and others, 2009, 2011; Olig and others, 2011), and evaluations of the potential for partial- and multiple-segment ruptures on the fault (e.g., Chang and Smith, 2002; DuRoss, 2008).

Brigham City Segment

Description of Surface Faulting

The Brigham City segment is the northernmost segment of the WFZ that has evidence of Holocene surface faulting. The surface trace of the segment is complex, and extends 36 km from North Ogden to Honeyville along the western base of the Wellsville Mountains (Personius, 1990) (figure 2). In general, scarp offset increases from several meters across Holocene geomorphic surfaces to several tens of meters across late Pleistocene surfaces. The southern terminus of the segment is at the Pleasant View salient (figure 2), which consists of complexly faulted late Pleistocene alluvial-fan deposits that shallowly bury bedrock on the hanging wall of the WFZ (Personius, 1990). East of the salient, a 1.5-km-wide left step separates the BCS from the northern Weber segment (WS) (Personius, 1990; Nelson and Personius, 1993). The northern end of the BCS is marked by a range-front reentrant near Coldwater Canyon; there, scarps on Holocene to late Pleistocene surficial deposits form a zone of complex faulting that overlaps with the southern end of the Collinston segment (Personius 1990; Hylland, 2007b).

Vertical surface offsets measured from scarp profiles along the trace of the BCS range from about 1 to 40 m, depending on the age of the displaced geomorphic surface. Late Pleistocene surfaces include alluvial-fan remnants at the ends of the segment that predate the Bonneville lake cycle, which occurred between about 30 and 12 ka (Oviatt and others, 1990, 1992; Oviatt, 1997; Godsey and others, 2005). Personius (1990) indicated 28–40 m of surface offset across these surfaces, which may be 100–200 kyr old. Latest Pleistocene surfaces include Lake Bonneville nearshore sands and gravels as well as alluvial fans graded to the Bonneville highstand shoreline (about 18–17 ka; Oviatt, 1997) and to the Provo shoreline (about 17–14 ka; Oviatt, 1997; Godsey and others, 2005). Surface offsets on these latest Pleistocene surfaces generally increase southward from 4–15 m along the northern half of the segment to 10–25 m south of Brigham City (Box Elder Canyon; Personius, 1990). Early to middle Holocene alluvial fans that postdate the Bonneville and Provo shorelines have less than 5 m of surface offset (Personius, 1990); however, these measurements are mostly limited to the Brigham City area. The youngest, late(?) Holocene alluvial-fan surfaces are faulted only along the southern third of the segment (Personius, 1990) and have 1–2 m of surface offset (this study).

Previous Paleoseismic Investigations

At least six Holocene earthquakes have occurred on the BCS (figure 3, table 1). These data are from a modified gravel-pit exposure of a subsidiary fault trace on the Pleasant View salient at Pole Patch (Personius, 1991b), and from two paleoseismic trench sites near the center of the segment at Bowden Canyon (Personius, 1991a) and Box Elder Canyon (McCalpin and Forman, 2002). However, of the six earthquakes, only three earthquakes—at about 6.0 ka, 4.7 ka, and 3.5 ka—correlate among the sites (table 1). Importantly, at the time of this study, paleoseismic information for the youngest BCS earthquake at about 2.1 ka was derived from a single site—Box Elder Canyon. Using these data, the mean recurrence interval since the mid Holocene for the BCS is about 1.3 ± 0.1 kyr.

The Pole Patch trench was excavated in 1985 along a pre-existing exposure of a northeast-trending (down-to-the-northwest) normal fault at the boundary between the BCS and Weber segment (Pleasant View salient; figure 3) (Personius, 1991b). The trench revealed evidence of three surface-faulting earthquakes: two postdating the Bonneville highstand, and a

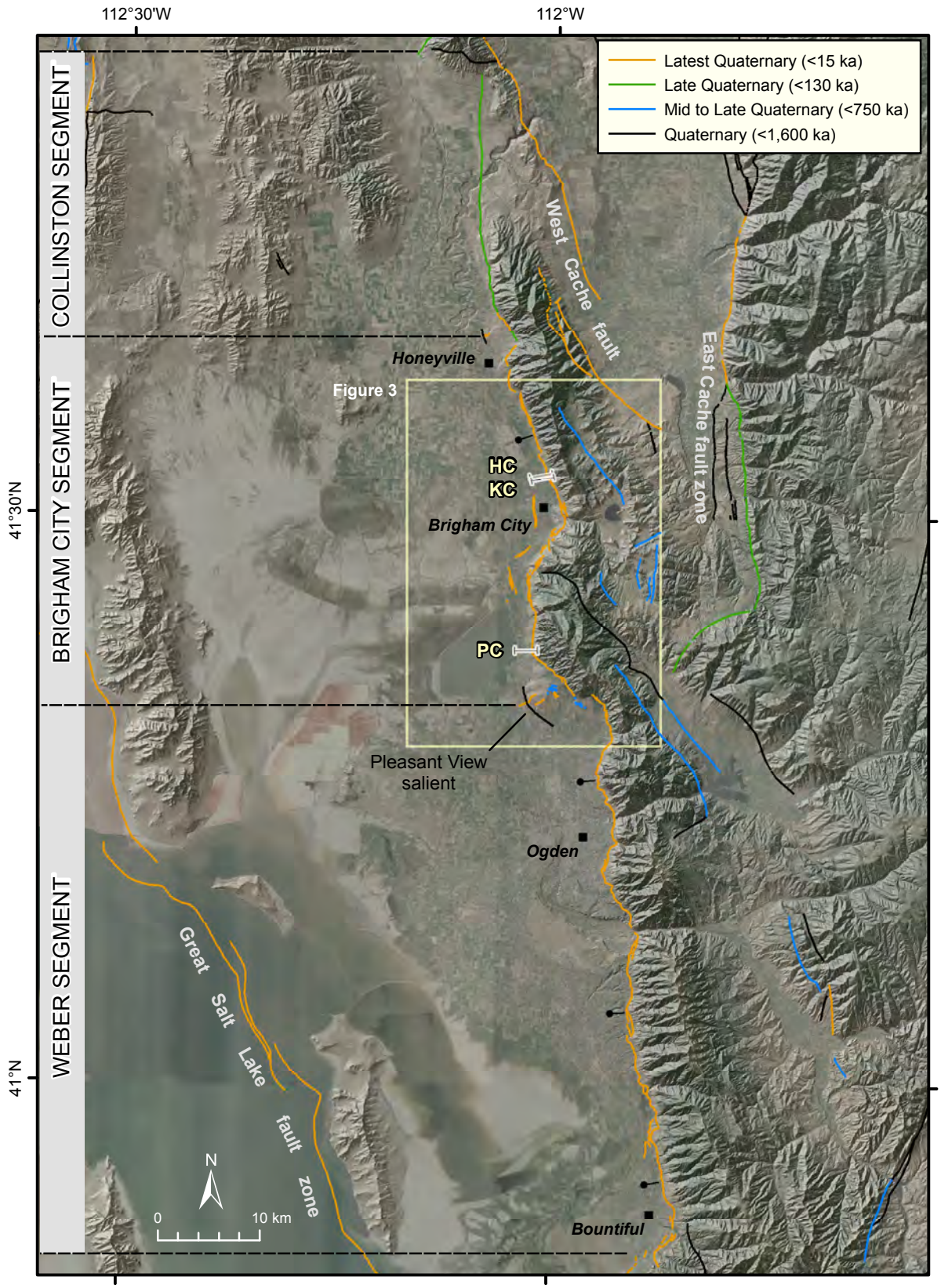

Figure 2. *Surface traces of the Collinston, Brigham City, and Weber segments of the Wasatch fault zone (WFZ), showing the Hansen Canyon (HC), Kotter Canyon (KC), and Pearsons Canyon (PC) trench sites. Trace of the WFZ and other Quaternary faults from Black and others (2003); ball and bar on down-thrown side. Base maps: 2006 National Agricultural Imagery Program (NAIP) aerial photography (U.S. Department of Agriculture [USDA], 2008) and 30-m DEM (UAGRC, 2012).*

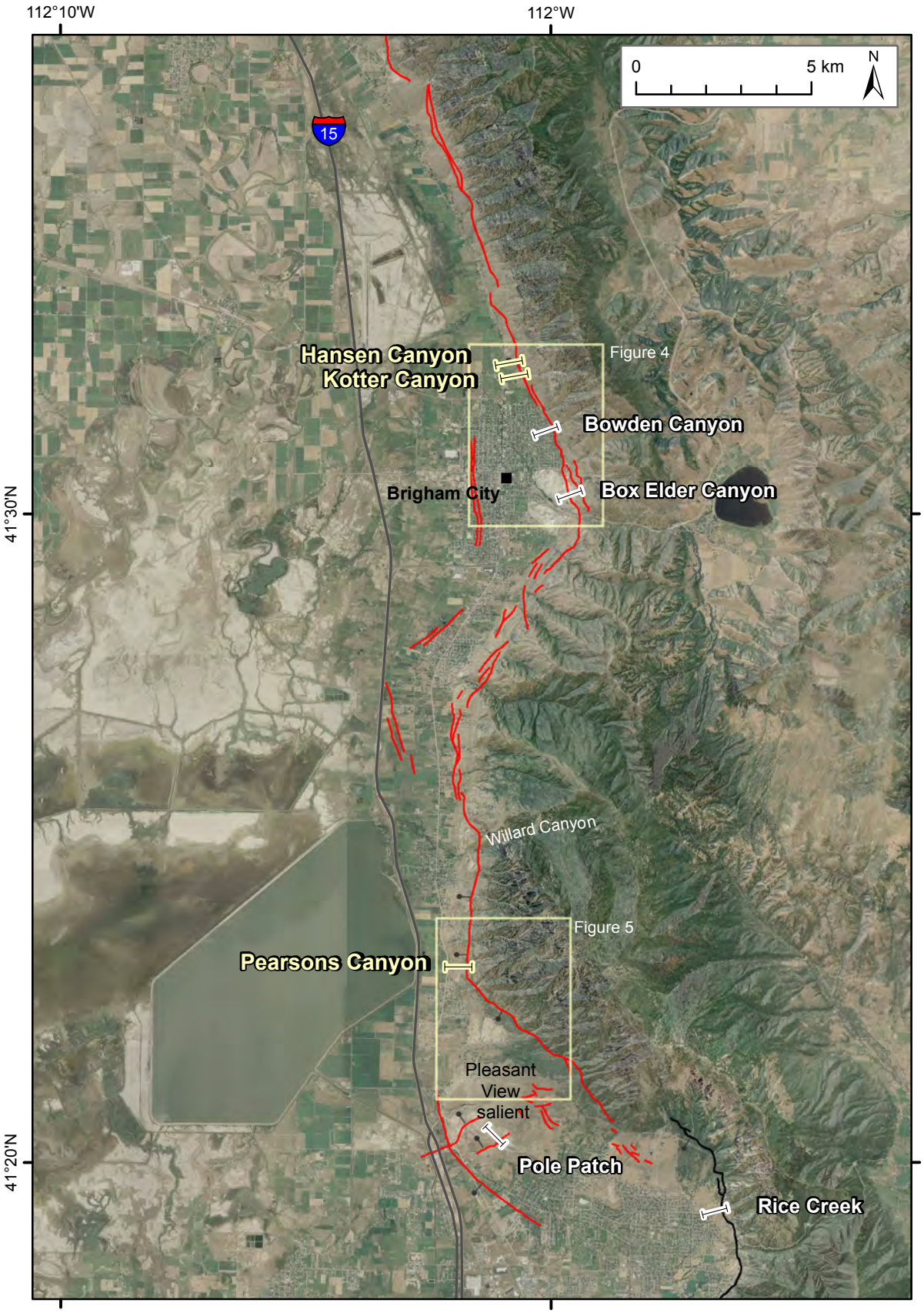

Figure 3. *Brigham City segment of the WFZ (red), showing paleoseismic sites (yellow – this study; white – previous studies); the northern Weber segment of the WFZ is shown in black (Black and others, 2003). Base maps: 2006 NAIP aerial photography (USDA, 2008) and 10-m DEM (UAGRC, 2012).*

most recent earthquake (MRE) that occurred prior to 4.5 ± 0.7 ka based on a radiocarbon (^{14}C) age for soil organics sampled from a tectonic crack. Personius (1991b) calibrated the age and used assumptions about the mean residence time of soil organics to estimate a time of 4.6 ± 0.5 ka for the MRE at the site (table 1). The older two earthquakes were only broadly constrained between the age of the MRE and the Bonneville Flood (about 18 ka, based on Oviatt [1997]). About 1.5–2.5 m of vertical displacement occurred in each of the older two Pole Patch earthquakes, compared to about 0.7–1.3 m in the MRE (table 1).

At the Bowden Canyon site, Personius (1991a) excavated a single trench in 1986 across an 8-m-high scarp and found evidence of three surface-faulting earthquakes younger than the mid-Holocene. The MRE occurred at about 3.6 ± 0.5 ka based on minimum- and maximum-limiting ^{14}C ages of 1.2 ± 0.1 ka and 3.6 ± 0.3 ka, respectively, from soil organics. The penultimate earthquake occurred at 4.7 ± 0.5 ka based on two maximum soil ^{14}C ages of 4.6 ± 0.6 ka and 4.7 ± 0.6 ka (Personius, 1991a). These ages provide a minimum constraint on the oldest earthquake, which Personius (1991a) estimated at 5–7 ka. Personius (1991a) estimated about 2.5 m of vertical displacement in each of the older two earthquakes and 1.0 m in the MRE (table 1). Personius (1991a) did not find evidence for an event younger than about 3.6 ka and noted the long elapsed time since the MRE compared to the relatively short (1–2 kyr) intervals between the three events. However, the Bowden Canyon trench exposed complicated structure and stratigraphy, including multiple fault zones and extensive erosional unconformities, and Personius (1991a, p. 6) noted the possible presence of an additional buried soil in the colluvial sequence, all of which could allow for an alternative interpretation of two post-3.6 ka earthquakes.

At the Box Elder Canyon site, McCalpin and Forman (2002) excavated 14 trenches (in 1992–93) across seven subparallel scarps in a complex (300-m-wide) fault zone formed on a Lake Bonneville delta graded to the Provo-phase shoreline (about 14–18 ka). McCalpin and Forman (2002) interpreted six earthquakes younger than ~8.5 ka at the site (table 1) based on trench mapping and ^{14}C and thermoluminescence (TL) ages. Three of these earthquakes, at about 3.4 ka, 4.7 ka, and 6.0 ka, correspond well with events identified at Pole Patch and Bowden Canyon (table 1). Importantly, McCalpin and Forman (2002) reported an MRE at 2.1 ± 0.1 ka, based on a maximum TL age of 2.0 ± 0.5 ka, maximum ^{14}C soil ages ranging from 1.8 to 2.8 ka, and a minimum ^{14}C soil age of 1.4 ± 0.3 ka. The two youngest earthquakes at ~3.4 and 2.1 ka had minimum vertical displacements of 1.1 m and 0.5–1.2 m, respectively. Only poorly constrained minimum displacements were reported on account of the complex Provo-delta fault zone, which complicated the measurement of throw across individual scarps.

Why Trench the Brigham City Segment?

Of the five central WFZ segments, the BCS has the longest elapsed time since its most recent earthquake (~2.1 kyr), which is over 1.5 times its mean Holocene earthquake recurrence interval (~1.3 kyr). Thus the BCS has the highest time-dependent earthquake hazard of any WFZ segment (McCalpin and Nishenko, 1996; McCalpin and Forman, 2002; Wong and others, 2002). However, timing and displacement data for the 2.1-ka earthquake are limited to a single trench site at Box Elder Canyon. Furthermore, scarps on late Holocene surfaces suggest younger faulting along the southern one-third of the segment (Personius, 1990; this study). Thus, we excavated trenches at three sites to determine whether a surface-faulting earthquake younger than 2.1 ka occurred on the BCS. Obtaining a complete Holocene paleoseismic record for the segment is critical to understanding the segmentation of the northern WFZ, and for refining probabilistic earthquake-hazard assessments (e.g., in the USGS National Seismic Hazard Maps; Petersen and others, 2008), particularly for time-dependent estimates (e.g., Wong and others, 2002).

Table 1. *Summary of previous earthquake-timing data for the Brigham City segment.*

Earthquake[1]	Bowden Canyon[2]		Box Elder Canyon[3]		Pole Patch[4]	
	Timing (ka)	Displacement (m)	Timing (ka)	Displacement (m)	Timing (ka)	Displacement (m)
BC1	no evidence?		2.1 ± 0.1	> 0.5–1.2	no evidence	
BC2	**3.6 ± 0.5**	**1.0**	**3.4 ± 0.1**	**> 1.1**	no evidence	
BC3	**4.7 ± 0.5**	**2.5**	**4.7 ± 0.1**	-	**4.6 ± 0.5**	**0.7–1.3**
BC4	**5–7**	**2.5**	**6.0 ± 0.2**	-	two events >4.6 ± 0.5	1.5–1.8 2.2–2.5
BC5	not exposed		7.5 ± 0.4	-		
BC6	not exposed		8.5 ± 0.3	-		

[1] BC1 is most recent earthquake; bold text indicates earthquakes that correlate among trench sites.
[2] Bowden Canyon paleoseismic data summarized from Personius (1991a).
[3] Box Elder Canyon data from McCalpin and Forman (2002); older (pre-Holocene) earthquakes are not reported here.
[4] Pole Patch data from Personius (1991b).

Overview and Methods

In the spring of 2008, we sited trenches on the northern and southern parts of the BCS using 1:50,000-scale mapping by Personius (1990), our interpretation of low-sun-angle aerial photographs (Cluff and others, 1970; included in Bowman and others, 2009), and field reconnaissance. The Hansen Canyon and Kotter Canyon sites are on the northern half of the segment, about 3 km north of Brigham City (figure 4); the Pearsons Canyon site is near the southern end of the segment, 2.4 km northeast of South Willard (figure 5). These sites offered the best opportunity to investigate the youngest BCS earthquakes because they are both north and south of the previous paleoseismic trench sites on the segment, but several kilometers from the segment ends, and have small (~2-m-high) to moderate (~7-m-high) fault scarps formed on mid- to late Holocene alluvial-fan surfaces.

We mapped trench stratigraphy and structure at 1:20 scale and compiled photomosaics (1-m squares) of the main fault zones (plates 1–3). Using a total station (Trimble TTS 500), we measured the positions of markers (e.g., nails and flagging) along stratigraphic contacts and structures and projected the points to a vertical plane parallel to the average orientation of the south wall of each trench. We then plotted the points for each wall at 1:20 scale on gridded mylar and sketched in additional detail in the fault zones. The total station and assumed vertical plane were also used to set up a 1-m square grid on the trench walls, which provided a reference grid for constructing 1:20-scale photomosaics. Plate 1–3 includes maps and photomosaics of the exposures with a single coordinate system for each site (Hansen Canyon [HC], Kotter Canyon [KC], and Pearsons Canyon [PC]) referenced herein using horizontal (h-) and vertical (v-) meter marks (N – north trench, S – south trench). For example, the main fault in the Hansen Canyon south trench is at HC-S, h-16.1 m, v-6.3 m (plate 1). At each site, stratigraphic units are labeled from youngest (lowest number) to oldest (highest number). The unit numbers imply the correlation of units between trenches at a single site, but not between separate sites. Descriptions of stratigraphic units are included in plates 1–3 and in appendix A.

NUMERICAL DATING

Radiocarbon Dating

Sampling and Dating Strategy

Because we did not find macroscopic charcoal fragments in the trenches, we collected 25 about two-liter-sized bulk samples of organic-rich sediment from (1) the upper 5–10 cm of soil A horizons developed on alluvial-fan and scarp-colluvial deposits (e.g., sample PC-R1; PC-S, h-11.5 m, v-7.1 m; plate 3), (2) the matrix of scarp-derived colluvium (e.g., sample PC-R2; PC-S, h-11.8 m, v-7.4 m; plate 3), and (3) the organic-rich matrix of debris flows (e.g., sample PC-R7; PC-S, h-35.2 m, v-2.9 m; plate 3). These samples were submitted to Paleo Research Institute of Boulder, Colorado, for the separation and identification of plant macrofossils. Paleo Research Institute separated the samples into light (plant remains) and heavy (sediment) fractions following the floatation methods of Matthews (1979), and examined the light fractions for charcoal, seeds, and other plant remains under 10-70X magnification. Our preferred material for dating consisted of charred macrofossils of tree or shrub species local to the site that have short age spans (e.g., sagebrush; see Puseman and Cummings, 2005). For the A-horizon and scarp-colluvium samples, these locally derived charcoal fragments are less likely to have been transported to the site (and detrital in origin).

Our attempt to sample and date charcoal identified to family or genus level yielded poor results; only three of our bulk samples yielded fragments of identifiable charcoal (appendix B). The remaining 22 samples yielded collections of small, unidentified charcoal fragments, which we aggregated into samples of at least ~0.5 mg for radiocarbon (^{14}C) analysis. We submitted the identified and unidentified charcoal samples to Woods Hole Oceanographic Institute of Woods Hole, Massachusetts, for accelerator mass spectrometry ^{14}C dating. We report ^{14}C ages as the mean and two-sigma (2σ) uncertainty rounded to the nearest century in calendar-calibrated kilo-annum (thousand years) before 1950 (ka) (appendix C) using the Reimer and others (2009) terrestrial calibration curve applied in OxCal (version 4.1; Bronk Ramsey, 1995, 2001).

Sources of Dating Uncertainty

Charcoal samples derived from buried A horizons may yield anomalously young or old ^{14}C ages, despite having a known stratigraphic and structural context (Machette and others, 1992; McCalpin, 1996). Anomalously young ages (e.g., sample PC-R5; PC-S, h-34.6 m, v-2.9 m; plate 3) can result from charcoal that was separated from A-horizon samples containing young charcoal mixed by burrowing organisms or rootlets that decayed or burned in place. In contrast, anomalously old ages (e.g., sample PC-R3; PC-S, h-12.0 m; v-7.0 m; plate 3) generally indicate carbon reworked from soil or sediment that predates the sampled soil horizon. Charcoal can also have an inherited (inbuilt) age from the age of the plant when it burned. To minimize these potential dating uncertainties, we avoided sampling near heavily burrowed parts of the trench exposure, collected the uppermost part of the A horizons where possible to obtain the youngest charcoal accumulated in the soil prior to burial, and selected charcoal derived from plants having short age spans whenever possible.

Samples of colluvial- and debris-flow-matrix sediment may also yield anomalously young or old ages due to burrowed or detrital sediment, respectively. Detrital charcoal can have an inherited age from the elapsed time that it lay on the ground surface before being incorporated into a debris flow or transported by stream flow. For example, charcoal from

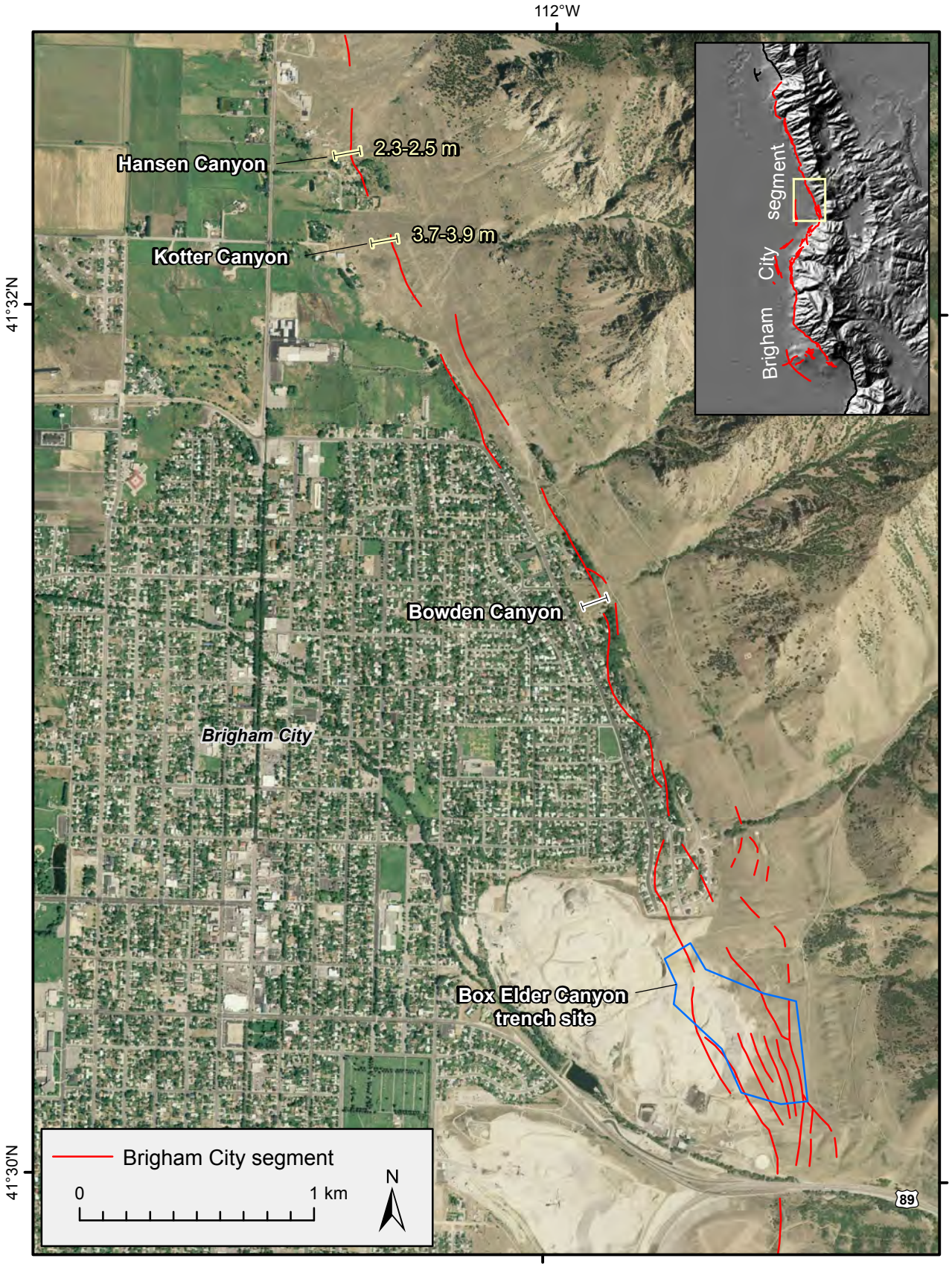

Figure 4. *Central Brigham City segment, showing vertical scarp offsets measured at the Hansen Canyon and Kotter Canyon sites (this study), and the Bowden Canyon and Box Elder Canyon trench sites (previous studies). Base maps: 2006 NAIP aerial photography (USDA, 2008) and 30-m DEM (inset map; UAGRC, 2012).*

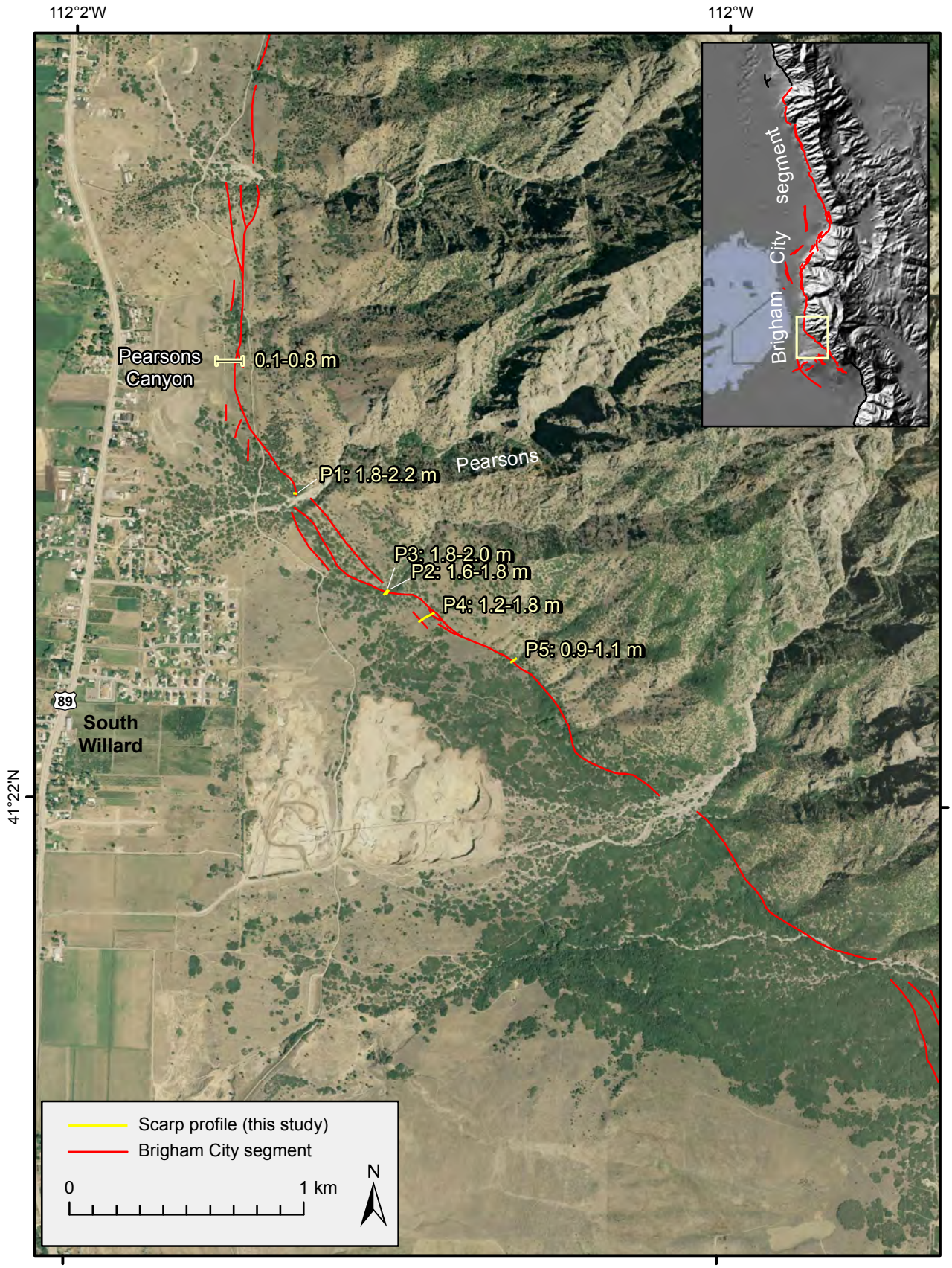

Figure 5. *Southern Brigham City segment, showing the Pearsons Canyon trench site and vertical surface offset measured from scarp profiles (P1–P5; this study). Base maps: 2006 NAIP aerial photography (USDA, 2008) and 30-m DEM (inset map; UAGRC, 2012).*

coarse, woody debris (e.g., a dead standing tree or snag) can have an inherited age of hundreds to possibly several thousands of years depending on the wood species, tree diameter, and decay rate (Harmon and others, 1986; Gavin, 2001). However, for the colluvial deposits, we assumed that the organic sediment sampled would (1) closely approximate the time of surface faulting because the organics were eroded from A horizons exposed by surface faulting, or (2) postdate the time of surface faulting if the charred organics were from A horizons developed on the post-earthquake colluvium. In contrast, we infer that charcoal ages from the debris-flow deposits approximate the time of deposition as they contain organic sediment likely stripped from surficial deposits (and A horizon sediment) during transport. However, the ages may also predate the time of deposition if the charcoal is detrital in origin or eroded from older deposits.

Luminescence Dating

Optically stimulated luminescence (OSL) dating relies on the cumulative dose of *in situ* natural radiation in sediment grains to estimate the last time when that sediment was exposed to sunlight (Huntley and others, 1985). Ideally, the sunlight exposure was sufficiently long (about 1 hour) during deposition to fully reset or zero any preexisting luminescence signal in the grains, and thus the luminescence age should represent the time that the sediment was deposited and buried (Aitken, 1994). If the sediment was not exposed to sunlight long enough (e.g., because of rapid deposition or the light-filtering effect of turbid water), then it may retain an inherited luminescence signal (Forman and others, 1991). In this case, the OSL age will be a maximum age for the deposit.

We collected three samples from the Kotter Canyon trench (appendix D) for conventional (multi-aliquot) OSL dating and submitted two of the samples (KC-L2 and -L3; plate 2) to the USGS Luminescence Dating Laboratory in Denver, Colorado. The sampled deposits consisted of discontinuous lenses of medium- to fine-grained and moderately to well-sorted sand in the alluvial-fan sediments. We measured the *in situ* dose of background radiation from potassium, thorium, and uranium isotopes using a gamma-ray spectrometer in the field; appendix D shows the sample saturation percent, total radiation dose rate, and equivalent dose.

We report OSL ages as the mean and 2σ uncertainty rounded to the nearest century in thousands of calendar years before the sample processing date (generally 2008). In discussing the ages, we do not account for the 58-yr difference in the OSL sample date (2008) versus the reference standard for ^{14}C (1950). This difference is minor compared to the large OSL age uncertainties (0.5–0.6 ka at 2σ), and is accounted for in later modeling of earthquake times in OxCal (discussed below).

OxCal Modeling

To evaluate earthquake timing and associated uncertainties, we used OxCal ^{14}C calibration and analysis software (version 4.1; Bronk Ramsey, 1995, 2001; using the IntCal09 calibration curve of Reimer et al., 2009). OxCal probabilistically models the timing of undated events (e.g., earthquakes) by weighting the time distributions of chronological constraints (e.g., ^{14}C and OSL ages and historical constraints) included in a stratigraphic model (Bronk Ramsey, 2008). The program generates a probability density function (PDF) for each event in the model, or the likelihood that an earthquake occurred at a particular time, using the chronologic and stratigraphic constraints and a Markov Chain Monte Carlo (MCMC) sampling method (Bronk Ramsey, 2008). For more detailed discussions of the application of OxCal modeling to paleoseismic data, see Lienkaemper and Bronk Ramsey (2009) and DuRoss and others (2011).

OxCal depositional models for the Hansen Canyon, Kotter Canyon, and Pearsons Canyon sites (appendix E) use stratigraphic ordering information, ^{14}C and OSL ages, and a historical constraint that no large surface-faulting earthquakes (M ~6.5+) have occurred since about 1847 to model the time distributions of earthquakes identified at the sites. For Hansen Canyon and Pearsons Canyon, we correlated depositional units between trenches and constructed a single OxCal model for each site. Where necessary, we removed numerical-age outliers using geologic judgment (knowledge of sediments, soils, and sample contexts), the degree of inconsistency with other ages in the model for comparable deposits (e.g., stratigraphically inverted ages), and an agreement index between the original (unmodeled) and modeled numerical ages (Bronk Ramsey, 1995, 2008). We report earthquake time ranges for each site as the mean and 2σ uncertainty in thousands of calendar years before 1950 (ka) rounded to the nearest century.

HANSEN CANYON SITE

At the Hansen Canyon trench site, we excavated two trenches across a west-facing, 4-m-high fault scarp (figure 6) on early to middle Holocene distal alluvial-fan deposits (Personius, 1990). We chose the site because of the moderate scarp height (which increases to the north and south), minimal scarp erosion (to the north, late Holocene or historical debris flows partially to fully conceal the scarp), and simple geometry, all of which are important to studying the most recent BCS earthquake. The trenches consisted of a 27-m-long north trench and 6-m-long south trench (plate 1).

Surface Offset

A 107 m-long profile across the Hansen Canyon site indicates 2.4 ± 0.1 m of vertical surface offset (figure 7). East of the scarp, the upper alluvial-fan surface is planar and slopes 5°–

7° southwest (230°–240°). In contrast, to the west, the lower surface slopes 1°–5° west-southwest (195°–205°) (figure 7). While this reduced slope could be partly explained by antithetic faulting, the topographic map for the site (plate 1) indicates that the slope is likely related to a 20–30-m-wide and less than 1-m-high alluvial-fan lobe (one or more debris flows) deposited on the down-thrown side of the fault scarp. Projecting the surface of the fan lobe toward the scarp yields a vertical surface offset of 2.3 m, compared to an offset of 2.5 m found by projecting the lower fan surface from west of the fan lobe (figure 7).

Trench Stratigraphy and Structure

The north and south trenches exposed both faulted and unfaulted alluvial-fan deposits and scarp-derived colluvium from a single earthquake (plate 1). The faulted fan deposits (units 3 and 4) consist of poorly sorted, 0.5- to greater than 1.5-m-thick, pebble- and cobble-rich debris-flow deposits that we differentiated on the basis of color and sorting. A 0.1–0.5-m-thick, brown, organic-rich A horizon (unit 3A; plate 1) is developed on unit 3. Scarp colluvium (unit 2) consists of a very poorly sorted deposit of silt, sand, and gravel that overlies the faulted soil unit 3A. In the north trench, unit 2 is less than 0.6 m thick and fills a 2.5-m-wide graben. In the south trench, unit 2 is wedge shaped, a maximum of 0.7 m thick, and overlies poorly sorted, sheared alluvial-fan sediment. In both trenches, unit 2 is overlain and locally modified by a post-faulting, massive, pebble to boulder, organic-rich debris flow (unit 1).

The Hansen Canyon trenches exposed simple to complex faulting. In the north trench, the main fault zone consists of a 1.0–2.5-m-wide zone of synthetic and antithetic faults (F2 to AF2). Zones of sheared sediment along the main down-to-the-west fault (F2) and antithetic fault zone (faults AF1–2) are 0.1–0.5 m wide. We also measured near-fault drag as far as 3 m east of fault F2, where the westward slope of the unit-3-4 contact increases from 5° to 20° (HC-N, h-14.0 m, v-8.0 m; plate 1). In the south trench, the WFZ is expressed as a narrow, less than 0.5-m-wide, near-vertical to slightly overturned (about 80° east-dipping) zone of sheared sediment with down-to-the-west displacement.

We measured 0.6–1.0 m of vertical, down-to-the-west stratigraphic displacement from a single earthquake. This estimate accounts for 0.7–1.0 m of displacement across the unit-3-4 contact in the north trench and 0.6–0.7 m in the south trench. In addition, we measured 0.8 m of displacement across the top of unit 3A in the north trench, projecting across the faulted graben (h-15.2–18.2 m; plate 1) where unit 3A is extensively faulted and possibly eroded. However, these unit 3–4 and 3A displacement values could be minima because of stratigraphic contacts affected by near-fault drag. Unit 3A is displaced approximately 1 m in the south trench, but has a limited exposure in the fault footwall. The maximum vertical surface offset of 2.5 m (profile HC-P1, figure 7) likely represents a reasonable maximum displacement for the site as it fully accounts for any near-fault drag.

Figure 6. *Photographs of the Hansen Canyon trench site (May 2008). (A) The north and south trenches across the Wasatch scarp (tripod positioned near base), which has about 2.4 m of vertical surface offset; view is to the east. (B) Fault zones exposed in the south walls of the trenches, showing faults F2–AF2, which correspond to labeling on plate 1.*

Four charcoal samples from unit-3A sediment and three from the matrix of unit 1 help constrain the timing of the earthquake. Ages of 4.3 ± 0.1 ka (2σ) (sample HC-R7; appendix C) and 4.7 ± 0.1 ka (HC-R8) for unit 3A in the south trench and 5.0 ± 0.2 ka (HC-R1) in the north trench provide a maximum limit. Charcoal from a fourth sample produced an additional maximum age of 6.8 ± 0.1 ka (HC-R2), but the sample likely included anomalously old (possibly detrital) charcoal. Charcoal from unit 1 yielded a minimum age of 2.1 ± 0.1 ka (HC-R5). Considering the significant difference between the minimum (~2 ka) and maximum (~5 ka) ages, the maximum ages may have an inherited age component from detrital charcoal. Two additional samples of the unit-1 matrix yielded minimum ages of 0.7 ± 0.1 ka (HC-R9) and 0.4 ± 0.2 ka (HR-R6), which possibly reflect the incorporation of younger soil sediment (and charcoal) into the colluvium by bioturbation.

Paleoseismology of the Hansen Canyon Site

The most recent earthquake at the Hansen Canyon site occurred at 3.1 ± 1.3 ka, or 2.1–4.2 ka using the 5th–95th percentile range from the OxCal model (figure 8), and had 0.6–2.5 m of displacement (table 2). We prefer the 5th–95th range over the mean ± 2σ because the broad earthquake-timing PDF (figure 8) does not show central tendency (*i.e.*, is uniformly distributed). The earthquake occurred after the A-horizon developed on unit 3 (unit 3A) and before deposition of debris-

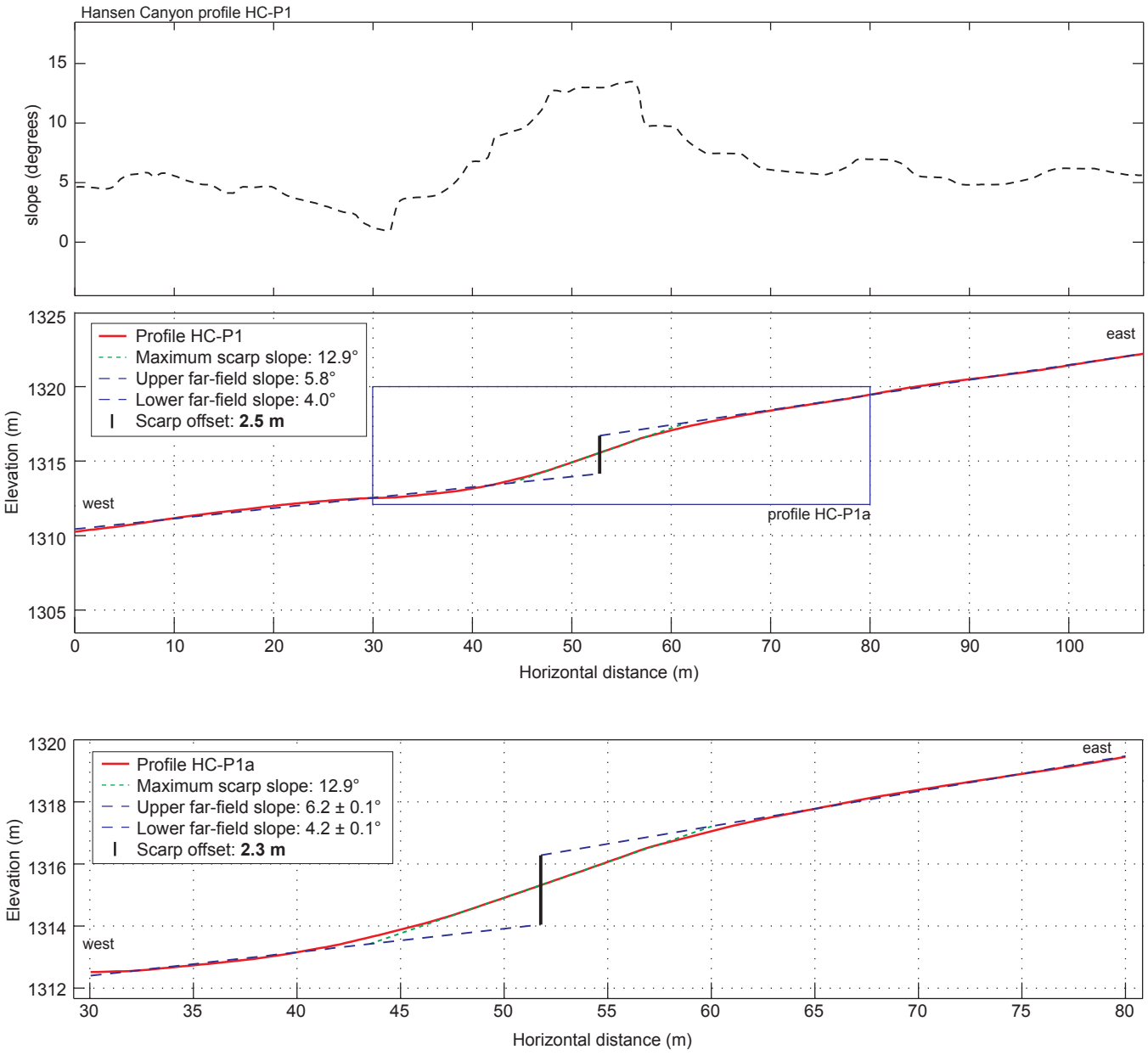

Figure 7. *Surface slope and scarp offset at the Hansen Canyon site based on profile HC-P1 (see plate 1 for location). Profile HC-P1a is a 50-m long subset of HC-P1 centered on the fault scarp.*

flow unit 1 at 2.1 ka (HC-R5). Charcoal from unit 3A indicates a maximum earthquake time of 4.3–5.0 ka (HC-R1, -R7, and -R8); however, these samples, as well as the 6.8-ka charcoal from sample HC-R2, are likely detrital in origin, and thus may have an unknown inherited age. We included the young (0.4–0.7 ka) ages for debris-flow unit 1 (HC-R6 and -R9 in the OxCal model); although these samples may have contained younger (near modern) soil sediment mixed by bioturbation, the soil ages nevertheless provide a minimum (albeit poor) limit on the time of the earthquake.

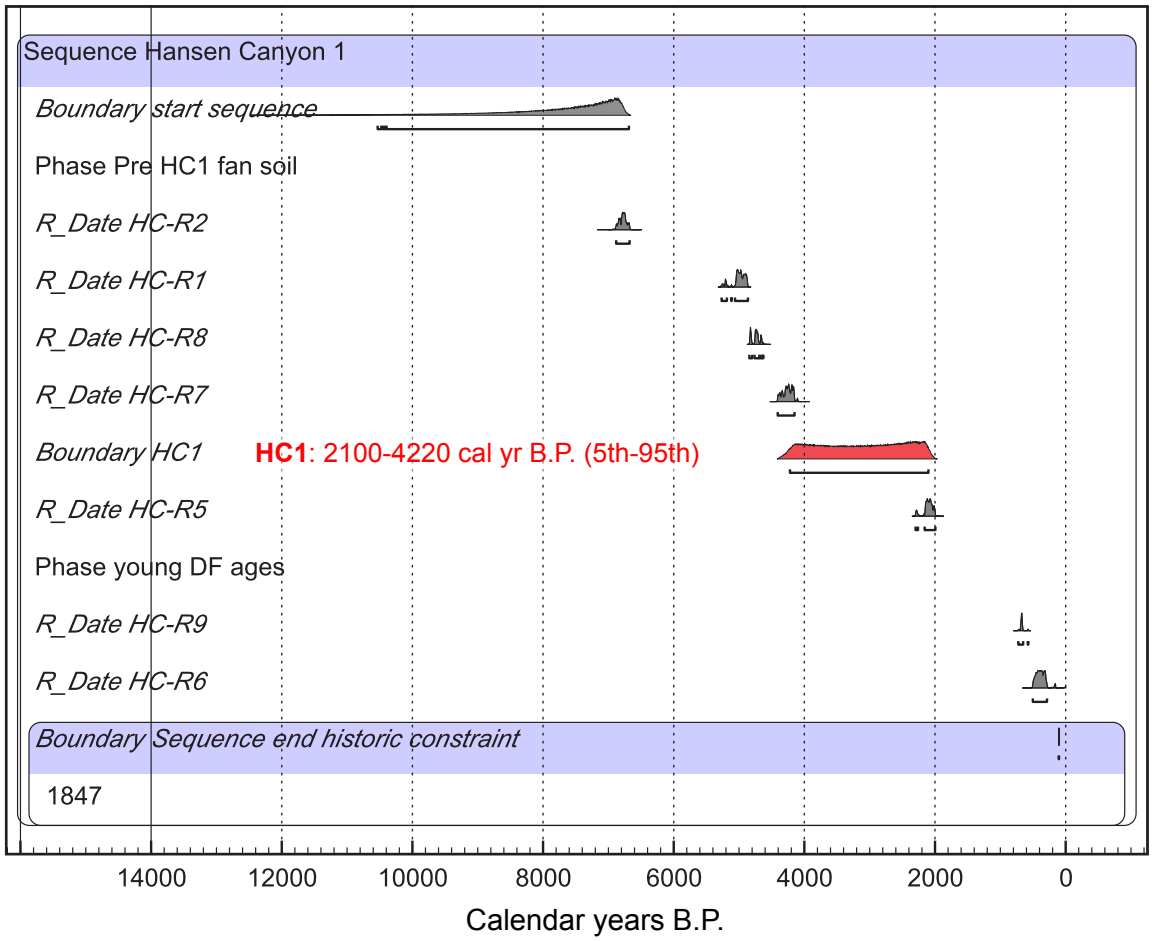

Figure 8. *OxCal model for the Hansen Canyon site, showing stratigraphic ordering of ^{14}C ages (appendix C) and a probability density function (PDF) for the most recent earthquake (HC1). Constructed using OxCal version 4.1 (Bronk Ramsey, 1995, 2001) and the IntCal09 radiocarbon calibration curve (Reimer and others, 2009). Brackets below PDFs indicate 2σ time ranges.*

Table 2. *Earthquake-timing, displacement, and slip-rate data for the Hansen Canyon, Kotter Canyon, and Pearsons Canyon sites.*

Earthquake	Earthquake time (cal yr B.P.)[1]		Recurrence (yr)[2]		Vertical displacement (m)[3]				Inter-event slip rate (mm/yr)[4]	
	Mean	±2σ	Mean	Min–Max	Trench	Surface	Pref.	Min–Max	Pref.	Min–Max
HC1	**3140**	**1320**	-	-	0.6–1.0	2.3–2.5	**1.6**	**0.6–2.5**	-	-
KC2	**3520**	**320**	-	-	1.9–2.3	3.7–3.9	**2.1**	**1.9–2.3**	-	-
KC1	**2450**	**280**	**1070**	**470–1670**	1.9–2.3	3.7–3.9	**2.1**	**1.9–2.3**	**2.0**	**1.1–4.9**
PC1	**1240**	**40**	-	-	0.5–0.8	0.1–0.8	**0.5**	**0.1–0.8**	-	-

[1] Mean earthquake time ± 2 sigma (2σ) based on OxCal models (appendix E); for HC1 we prefer the 5th–9th range of 2100–4220 cal yr B.P.
[2] Earthquake recurrence intervals, using mean and 2σ range (min–max) for earthquakes KC2 and KC1.
[3] Vertical displacement based on trench stratigraphy and structure (trench) and surface offset (surface) from scarp profiles. Pref. is midpoint displacement based on preferred min–max range, see text for discussion; for KC2 and KC1, range is one-half of minimum stratigraphic displacement (3.8–4.6 m).
[4] Closed seismic-interval vertical slip rate, using preferred displacement for KC1 and the inter-event recurrence interval for KC2–KC1.

Because we only identified evidence for one earthquake and the age of the alluvial-fan deposits is complicated by detrital charcoal, we were unable to determine earthquake-recurrence-interval or slip-rate estimates for the site.

KOTTER CANYON SITE

The Kotter Canyon trench site is about 0.5 km south of the Hansen Canyon site, where a west-facing, 8-m-high scarp displaces early to middle Holocene alluvial-fan deposits (Personius, 1990) (figure 9). We chose this site because (1) the fault displacement appeared to be concentrated on a single scarp, and (2) a nearby fault-trenching investigation conducted prior to construction of a housing development revealed a simple fault zone (Bill Black, Western GeoLogic, written communication, 2007). North and south of the site, the scarp is either modified or completely buried by late Holocene(?) debris flows. We excavated a 37-m-long trench that exposed evidence for two earthquakes.

Surface Offset

Two scarp profiles at the Kotter Canyon site indicate 3.7–3.9 m of vertical surface offset (figure 10). A long (>300-m-long) profile (KC-P1) indicates 3.8 ± 0.1 m of surface offset based on far-field surfaces sloping 7° to 10°. A second, shorter profile (KC-P2) parallel to the trench (plate 2) shows 3.7 m of vertical offset.

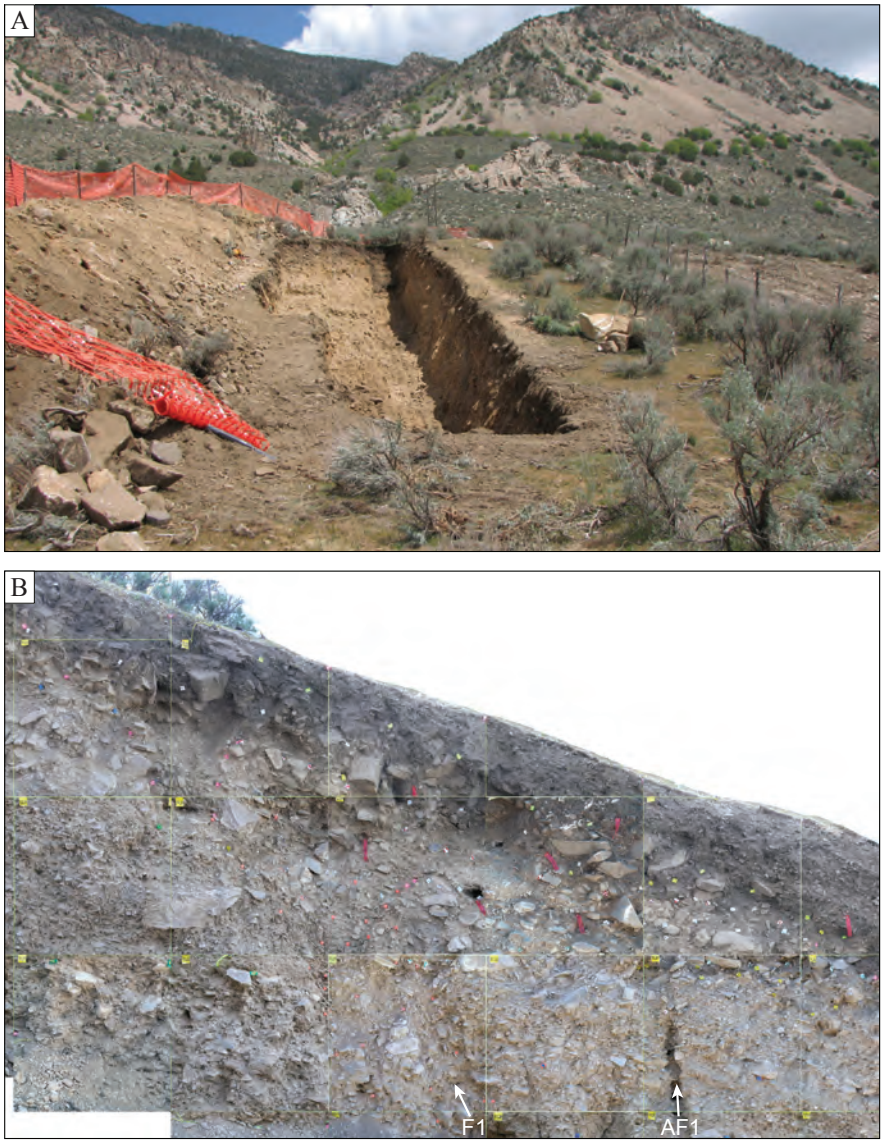

Figure 9. *Photographs of the Kotter Canyon trench site (May 2008). (A) View east toward the Kotter Canyon site, showing the Wasatch fault scarp, which has about 3.8 m of vertical surface offset. (B) Photomosaic of the fault zone exposed in the south wall, showing faults F1 and AF1, which correspond to labeling on plate 2; grid spacing is 1 m.*

Trench Stratigraphy and Structure

The Kotter Canyon trench exposed both faulted and unfaulted alluvial-fan deposits and scarp colluvium from two surface-faulting earthquakes (plate 2). The faulted fan deposits (unit 4) consist of pebble to boulder gravels that form subunits 4a to 4e, which are less than 1.4 m thick where fully exposed. On the upthrown side of the fault, unit 4 is moderately well stratified and dips 4°–8° west; however, on the down-thrown side, unit 4 dips 14°–26° west and has more abrupt lateral facies changes. Unit 4 is faulted down-to-the-west and overlain by poorly sorted, scarp-derived colluvium (unit 3) deposited after the older of the two earthquakes. Unit 3 tapers to the west from 0.7 m adjacent to the main fault zone (F1) to about 0.2 m in a 2.7-m-wide graben between faults F2 and AF2. Unit 3 thickens to about 0.5 m on the down-thrown side of fault AF2. Poorly sorted scarp colluvium associated with the most recent earthquake (unit 2) overlies unit 3. Unit 2 has a more pronounced wedge shape, with a maximum thickness of 1.4 m in the main fault zone and 1.0 m in the graben between F2 and AF2. An unfaulted, massive, pebble- and organic-rich debris-flow deposit (unit 1) is more than 0.7 m thick and overlies both units 2 and 4a.

Organic-rich A horizons consisting chiefly of silt and sand are developed on units 2, 3, and 4 (plate 2). The A horizon on unit 4 (4aA) is 0.2–0.5 m thick on both the upthrown and down-thrown sides of the fault zone, but is not developed on the fan deposits (unit 4a) exposed below scarp-colluvial unit

3. This relation suggests that the older earthquake occurred shortly after deposition of unit 4a, before any soil developed. The A horizons on units 3 (3A) and 2 (2A) are both about 0.2–0.5 m thick. These soils are continuous in the main fault zone (F1 to AF1); however, in the graben, unit 3A was more difficult to differentiate from the unit-4a matrix, and thus is mapped as more laterally discontinuous. Outside of the fault zone, unit 2A merges with unit 4aA.

The Kotter Canyon fault zone is as much as 13 m wide (faults F1 to F3); however, most displacement occurred in a 7-m-wide main fault zone between faults F1 and AF2 (KC, h-19–26 m; plate 2). The main fault zone includes a 0.7-m-wide zone of complex shearing adjacent to the main fault (F1; KC, h-19 m, v-11 m; plate 2) and a 2.7-m-wide graben between faults F2 and AF2 (KC, h-23.8-25.5 m; plate 2). Additional synthetic and antithetic faults that bound blocks of steeply west-dipping (14°–26°) fan gravel (unit

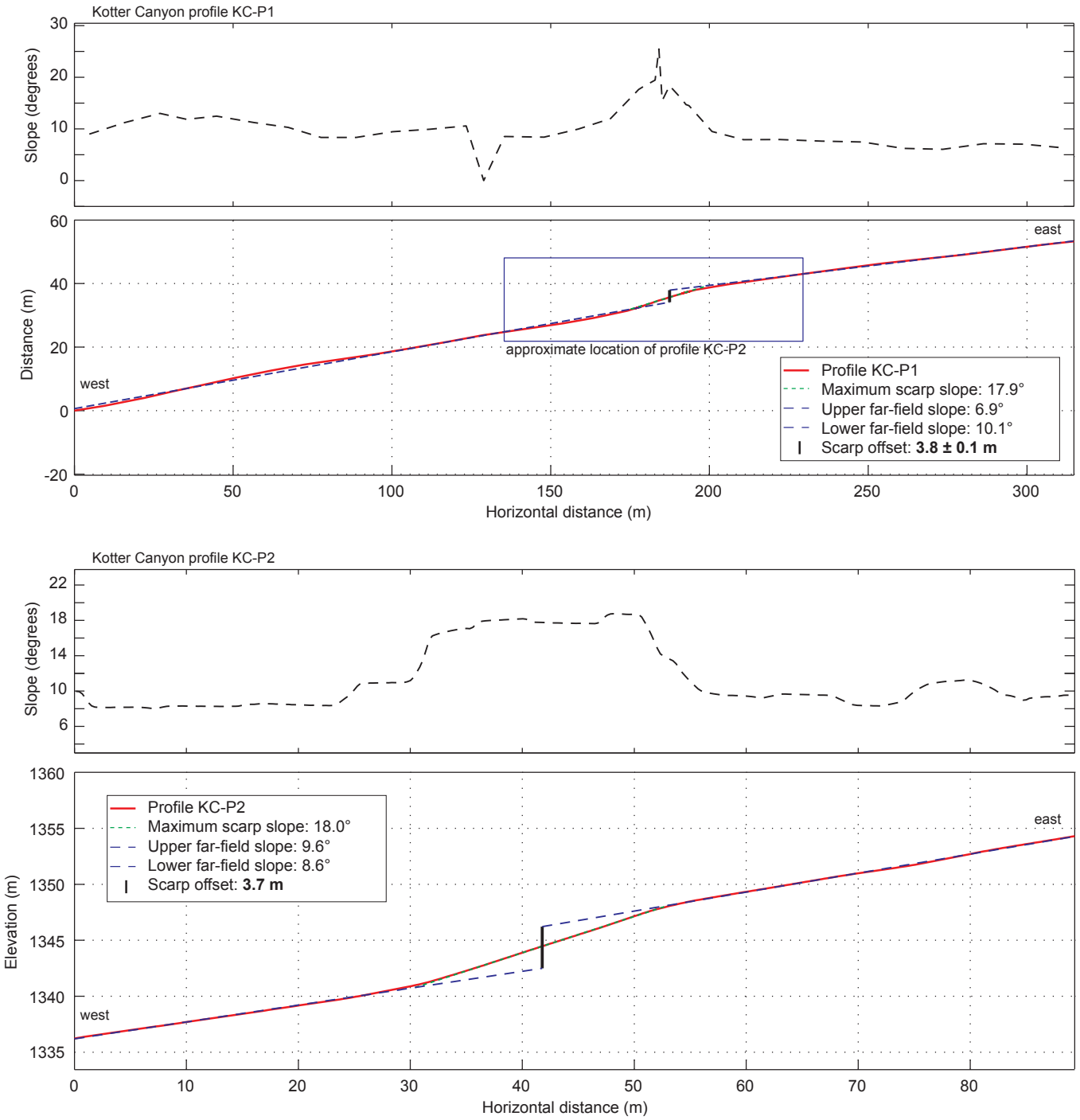

Figure 10. *Surface slope and scarp offset at the Kotter Canyon site based on profiles KC-P1 and -P2 (see plate 2 for location).*

4) are as much as 5 m west of fault AF2 (between faults F2 and F3; KC, h-24–31 m; plate 2) and have individual displacements less than about 0.5 m.

We estimate 1.9–2.3 m of average vertical displacement per event in the two surface-faulting earthquakes. Projecting the top of the alluvial-fan sequence (unit 4aA) toward fault F1 from the footwall and hanging wall yields only 1.3 m of displacement, which is a poorly constrained minimum estimate that does not account for the steep (14°–26°), fault-related dip of unit 4 on the hanging wall. Projecting the top and base of unit 4a from the footwall and westernmost part of the exposure to F1 yields lower-surface slopes of about 6° (projection of unit-4 contacts from 35–36 m; plate 2) to 8° (projection from 33–37 m; plate 2) and total vertical displacements of about 3.8–4.6 m, or 1.9–2.3 m per event. Scarp profile KC-P2 indicates about 3.8 m of total surface offset across the scarp (1.9 m per event). We consider this offset to be a good estimate of the total site displacement as both the upper and lower surfaces on the profile extend several meters outside of the fault zone (and fault scarp) and have similar surface slopes (about 9°). Thus, our preferred displacement per event is 1.9–2.3 m, based on both stratigraphic displacement and scarp offset. We chose not to apportion displacement according to the areas of the colluvial wedges because the complex hanging-wall faulting could have occurred in one or both earthquakes and would have affected per-event surface offset and scarp-colluvium generation.

OSL and ^{14}C ages constrain the timing of the two earthquakes. OSL ages of 3.6 ± 0.5 ka (2σ) (KC-L1) and 3.9 ± 0.6 ka (KC-L3) (appendix D) on fine sand and silt (unit 4c) from both the hanging wall and footwall of fault F1 support the correlation of unit 4 across the fault, and provide a maximum time for both earthquakes. We used ^{14}C dating to determine the age of seven samples of charcoal fragments from A horizons on scarp colluvial units 2 and 3, and from the matrix of debris-flow unit 1 (appendix C). Three samples of unidentified charcoal from soil unit 3A yielded ages of 2.3 ± 0.4 ka (KC-R11), 3.3 ± 0.1 ka (KC-R8), and 5.3 ± 0.3 ka (KC-R3). However, the 5.3-ka sample (KC-R3) likely contained anomalously old (possibly detrital) charcoal considering the 3.6–3.9-ka age of the OSL samples. Unidentified charcoal from unit 2A yielded an age of 2.5 ± 0.3 ka (KC-R4), which corresponds well with the youngest age (2.3-ka; KC-R11) for unit 3A. Charcoal from a single sample of unit 1 yielded two ages: numerous unidentified charcoal fragments yielded an age of 0.4 ± 0.1 ka (KC-R7a), and a single fragment of unidentified vitrified plant tissue produced an age of 5.2 ± 0.2 ka (KC-R7b). An additional sample of unit 1 yielded charcoal fragments with an age of 0.6 ± 0.1 ka (KC-R6). Considering the age differences between these samples, the ~0.5-ka ages (KC-R7a and -R6) likely better reflect the age of unit 1 as opposed to the ~5-ka sample (KC-R7b), which is likely derived from detrital charcoal incorporated into the debris flow.

Paleoseismology of the Kotter Canyon Site

Two earthquakes occurred at Kotter Canyon after deposition of alluvial-fan unit 4. Earthquake 2 (KC2) occurred after 3.6–3.9 ka, based on OSL ages for unit 4c, and before the 3.3 ka charcoal age for the A horizon developed on unit 3. These limiting ages in OxCal yield an earthquake time of 3.5 ± 0.3 ka for earthquake KC2 (figure 11, table 2).

The most recent earthquake (KC1) displaced unit 3, resulting in deposition of colluvial unit 2. The 2.3-ka age for unit 3A provides a maximum time for earthquake KC1 and the 2.5-ka charcoal age for unit 2 provides a minimum time. The 3.3-ka age for unit 3A in the graben provides a less well constrained maximum for the event. Including these ages in OxCal yields an earthquake time of 2.5 ± 0.3 ka (figure 11, table 2). We included the stratigraphically consistent ages of about 0.5 ka for unit 1 (samples R6 and 7a), but excluded the anomalously old age for unit 1 of about 5 ka (sample 7b), which is likely derived from detrital charcoal.

Using our mean and 2σ time ranges for earthquakes KC2 and KC1, the recurrence interval at Kotter Canyon is 1.1 kyr with a 2σ range of 0.5–1.7 kyr (table 2). The vertical slip rate is about 2.0 mm/yr, with a 2σ range of 1.1–4.9 mm/yr, using the 1.9–2.3-m average displacement for earthquake KC1 divided by the KC2–KC1 interval that precedes it. However, the potentially large slip rate of ~5 mm/yr, which stems from the relatively short (0.5-kyr) elapsed time between KC2 and KC1, is not representative of the average Holocene slip rate for the segment, which is ~1–2 mm/yr (Lund, 2005; using data from Personius, 1991a, 1991b).

PEARSONS CANYON SITE

The Pearsons Canyon site is about 6 km north of the southern end of the segment, where a 2-m-high, west-facing scarp and ~0.2-m-high, east-facing antithetic scarp are developed on a small (~100-m-wide) middle to late Holocene alluvial fan about 0.6 km north of Pearsons Canyon (figure 12). The Holocene alluvial-fan deposits postdate (are incised into) an older, about 15–20-m high scarp developed on hillslope colluvium overlying bedrock to the east (Personius, 1990). We chose the site because of the relatively small, simple scarps formed on the middle to late Holocene young alluvial-fan deposits, which likely recorded faulting from the most recent BCS earthquake. Scarps of similar height are present on late Holocene alluvial-fan surfaces to the south (at the mouth of Pearsons Canyon; figure 5), but are obscured by heavy oak vegetation or are formed on very coarse boulder fan deposits. We excavated two trenches: an 8-m-long north trench that crossed the main (down-to-the-west) scarp and a 32-m-long south trench that crossed both the main and antithetic scarps (plate 3). Because of the relatively large size of the scarp on the hillslope deposits and the presence of small scarps on younger deposits (likely formed in the most recent earthquake), we did not trench the 15–20-m high scarp.

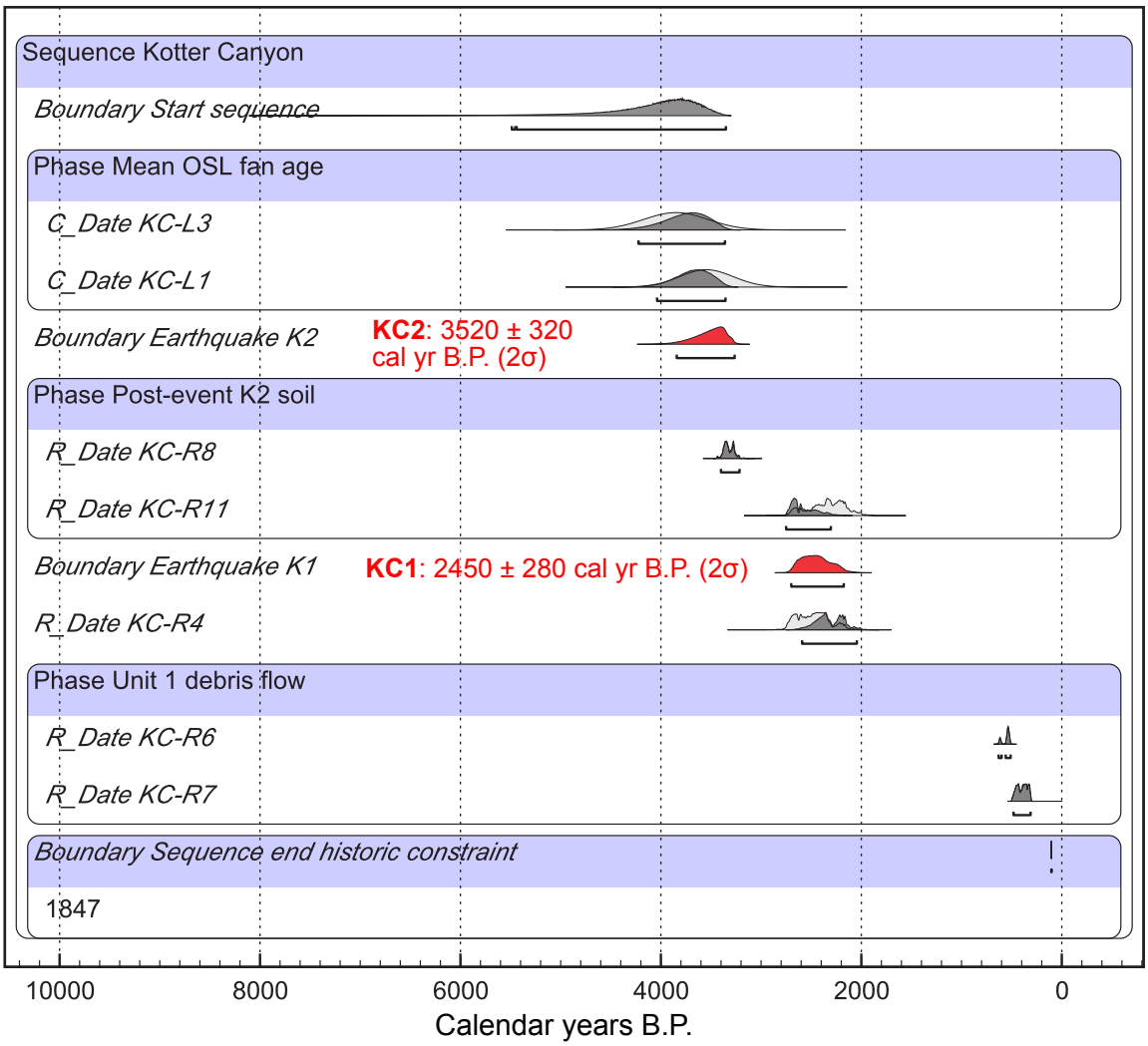

Figure 11. *OxCal model for the Kotter Canyon site, showing stratigraphic ordering of ^{14}C and OSL ages (appendices C and D) and probability density functions (PDFs) for earthquakes KC2 and KC1. Constructed using OxCal version 4.1 (Bronk Ramsey, 1995, 2001) and the IntCal09 radiocarbon calibration curve (Reimer and others, 2009). Brackets below PDFs indicate 2σ time ranges.*

Surface Offset

A ~50-m-long scarp profile measured across the Pearsons Canyon site indicates 0.1–0.8 m of net vertical surface offset (figure 13). The minimum offset (0.1 m) is based on the minimum main-scarp offset (0.7 ± 0.1 m) minus the maximum antithetic-scarp offset (0.4 ± 0.1 m), whereas the maximum offset (0.8 m) assumes that the main-scarp offset is a reasonable maximum for the site. Projecting the surface on the upthrown (west) side of the antithetic scarp toward the main scarp does not yield a surface offset due to a change in surface slope from 16° east of the main scarp to 12° west of the antithetic scarp.

Trench Stratigraphy and Structure

The north and south trenches exposed faulted alluvial-fan gravels (unit 3), scarp-derived colluvium related to a single earthquake (unit 2), and an unfaulted debris flow (unit 1) (plate 3). Unit 3 consists of poorly sorted, laterally heterogeneous pebble to boulder fan deposits (subunits 3a–3d) that are individually less than 1.6 m thick and together form a complex, interbedded package of fan gravel. Scarp-colluvial unit 2 includes very poorly sorted silt, sand, gravel, and organics that buried a soil A horizon on unit 3 (3bA and 3dA). Unit 2 is less than 0.8 m thick along the main scarp and less than 0.3 m thick adjacent to the antithetic scarp. On the down-thrown (east) side of the antithetic scarp, a pebble- and organic-rich debris flow (unit 1) has locally buried unit 2 (PC, h-31–37 m).

Organic-rich A horizons are developed on the alluvial-fan surface (units 3aA, 3bA, and 3dA). Where exposed at the surface, the A horizons are 0.3–0.6 m thick; however, where faulted and buried by units 2 (PC-S, h-11.0–13.5 m) or 1 (PC-S, h-34.8–35.8 m), the A horizons are 0.2–0.4 m thick.

Synthetic and antithetic fault zones in the south trench have a net displacement of 0.5 m. The main fault zone consists of a 0.1–0.6-m-wide zone of sheared sediment along fault F1 and a 3-m-wide graben between faults F1 and AF1. The vertical displacement across the main fault zone is 1.0 m, determined by projecting the top of the alluvial fan (top of unit 3aA) toward fault F1. The displacement between the unit 3c–3d contact in the footwall and the unit 3c–3d to 3b–3d contact in the hanging wall is 1.7 m; however, this value exceeds the surface offset and may indicate downcutting of unit 3c into 3d on the hanging wall, similar to the unit 3b–3c–3d contact at h-15–18 m (PC-S; plate 3). About 23 m west of fault F1, an antithetic fault (AF2) displaces unit 3 0.5 m down to the east based on projections of the tops of unit 3dA (footwall) and unit 3aA (hanging wall) toward AF2 (PC-N, h-21.9 m; PC-S, h-11.5–13.5 m; plate 3).

Faulting in the north trench consists of a single 0.1–0.2-m-wide zone of sheared sediment along fault F1 that displaced the unit 3b–3c contact 1.0–1.1 m down to the west. The north trench did not expose the antithetic fault zone; however, assuming at least 0.3 m of antithetic displacement (based on scarp profile PC-1), a reasonable maximum site displacement is 0.8 m.

Ten samples of A-horizon, scarp-colluvial-matrix, and debris-flow-matrix sediment yielded charcoal for ^{14}C dating (PC-R1 to -R9; appendix C). Three unidentified and conifer charcoal samples from unit 3bA have mean ages between 1.2 and 2.1 ka (PC-R4, -R8, and -R9) and provide a maximum time for the earthquake. Two additional maximum ages, including that for a fragment of juniper charcoal, are 3.2 ± 0.1 ka (PC-R1) and 5.4 ± 0.1 ka (PC-R3); however, these ages likely have an inherited component from recycled or detrital charcoal in the sampled sediment. One additional sample of unidentified charcoal from the A horizon (PC-R5) yielded an anomalously young age of 0.4 ± 0.1 ka and likely included bioturbated charcoal. Three samples of unidentified charcoal from the unit-2 scarp colluvium yielded minimum ages between 0.4 and 0.7 ka (PC-R6a and -R6b) and 1.2 ± 0.1 ka (PC-R2). The younger ages are likely from bioturbated charcoal in the sample, whereas the 1.2-ka age is consistent with the youngest A-horizon age (1.2 ka; PC-R9). Conifer charcoal from the matrix of debris-flow unit 1 produced a minimum age of 1.3 ± 0.1 ka (PC-R7).

Paleoseismology of the Pearsons Canyon Site

The most recent earthquake at the Pearsons Canyon site occurred at about 1.2 ka and had 0.1–0.8 m of displacement (including both stratigraphic-displacement and surface-offset estimates) (table 2). This time range considers the three overlapping minimum and maximum ages for the buried A horizon (about 1.2 ka), the scarp colluvium (about 1.2 ka), and the post-faulting debris flow (about 1.3 ka). Older ages (~3.2–5.4 ka) for charcoal from the A-horizon sediment likely have an inherited (detrital) component, whereas the younger ages (less than 0.7 ka) likely reflect bioturbated charcoal in the colluvial samples. Conifer charcoal from the A horizon provides a less well constrained maximum age of 1.8 ka. Including these ^{14}C ages in OxCal yields a mean and 2σ range

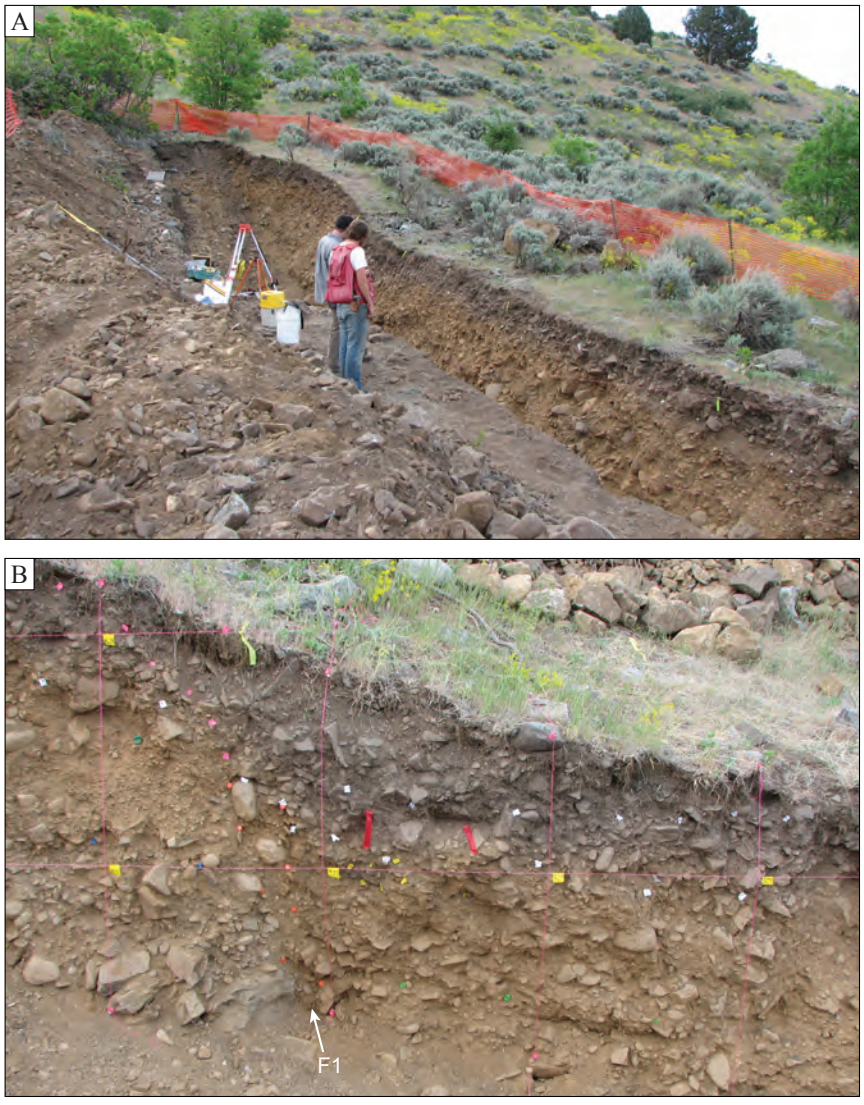

Figure 12. *Photographs of the Pearsons Canyon trench site (May 2008). (A) The south trench of the Pearsons Canyon site; tripod is positioned near the base of the Wasatch fault scarp, which has less than 1 m of vertical surface offset. View is to the southeast. (B) The fault zone exposed in the south wall of the north trench; fault F1 corresponds to labeling on plate 3. Red flags indicate locations of radiocarbon samples.*

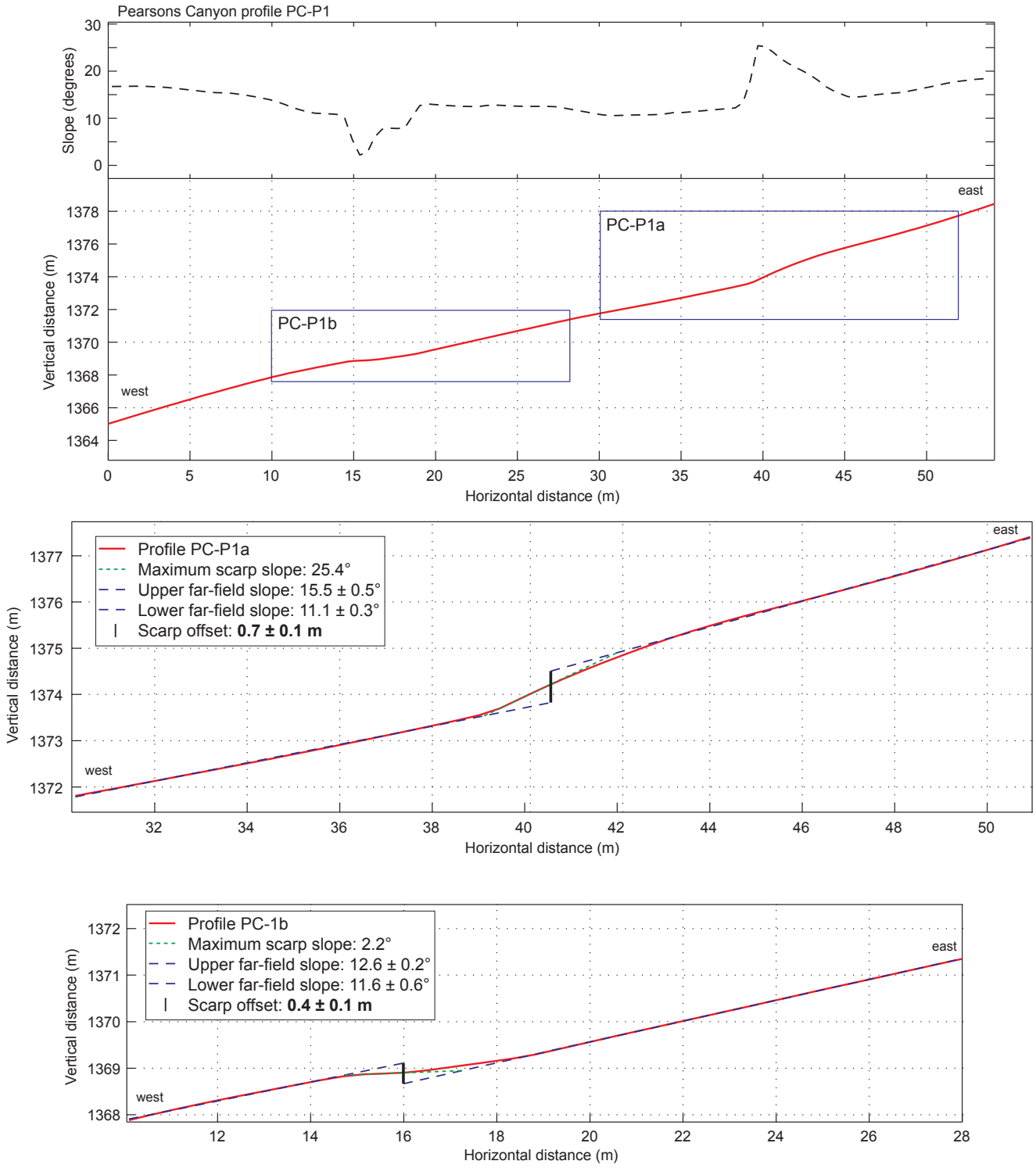

Figure 13. *Surface slope and scarp offset at the Pearsons Canyon site based on profile PC-P1 (see plate 3 for location). Profiles PC-P1a and PC-P1b are subsets of PC-P1 showing the main (west facing) and antithetic (east facing) fault scarps, respectively.*

of 1.2 ± 0.04 ka (figure 14). Because we only identified evidence for one earthquake and the age of the alluvial-fan deposits is poorly constrained, we were unable to determine earthquake-recurrence-interval or slip-rate estimates for the site.

PALEOSEISMOLOGY OF THE BRIGHAM CITY SEGMENT

Most Recent Earthquake on the Brigham City Segment

Paleoseismic data from Box Elder Canyon (McCalpin and Forman, 2002), Hansen Canyon, and Kotter Canyon demonstrate that the most recent earthquake on the main (north-central) BCS occurred before 2 ka (figure 15). The Hansen Canyon earthquake is poorly constrained to 2.1–4.2 ka; however, 0.5 km to the south, the Kotter Canyon site yielded a narrower earthquake range of 2.2–2.7 ka (2.5 ± 0.3 ka). These data are consistent with the five Box Elder Canyon luminescence and ^{14}C ages that constrain the most recent earthquake to a mean of 2.1 ± 0.1 ka (McCalpin and Forman, 2002). The second (penultimate) Kotter Canyon earthquake occurred at 3.5 ± 0.3 ka, which corresponds well with the second event at Box Elder Canyon (3.4 ± 0.1 ka) and the most recent earthquake at Bowden Canyon (3.6 ± 0.5 ka) (Personius, 1991a). Displacements for the most recent event are constrained to 0.6–2.5 m at Hansen Canyon and 1.9–2.3 m at Kotter Canyon, which are consistent with the Box Elder Canyon estimate of >0.5–1.2 m for the most recent earthquake and >1.1 m for the second earthquake.

Trenches at Pearsons Canyon and scarp profiles measured in this study indicate that an earthquake younger than 2 ka occurred on the southern BCS. Earthquake timing at 1.2 ± 0.04 ka is based on overlapping ages from three depositional units exposed in the trenches that both postdate and predate the earthquake (figure 15). We measured 0.1–0.8 m of vertical displacement for the event; however, antithetic displacement and a westward-decreasing surface slope complicate the measurement. A post-2-ka earthquake on the southern BCS is consistent with our field reconnaissance. South of Pearsons Canyon, we found scarps on relatively young (late Holocene?) alluvial-fan surfaces, including scarps at the mouths of active, steep drainages. These scarps have 1–2 m of vertical surface

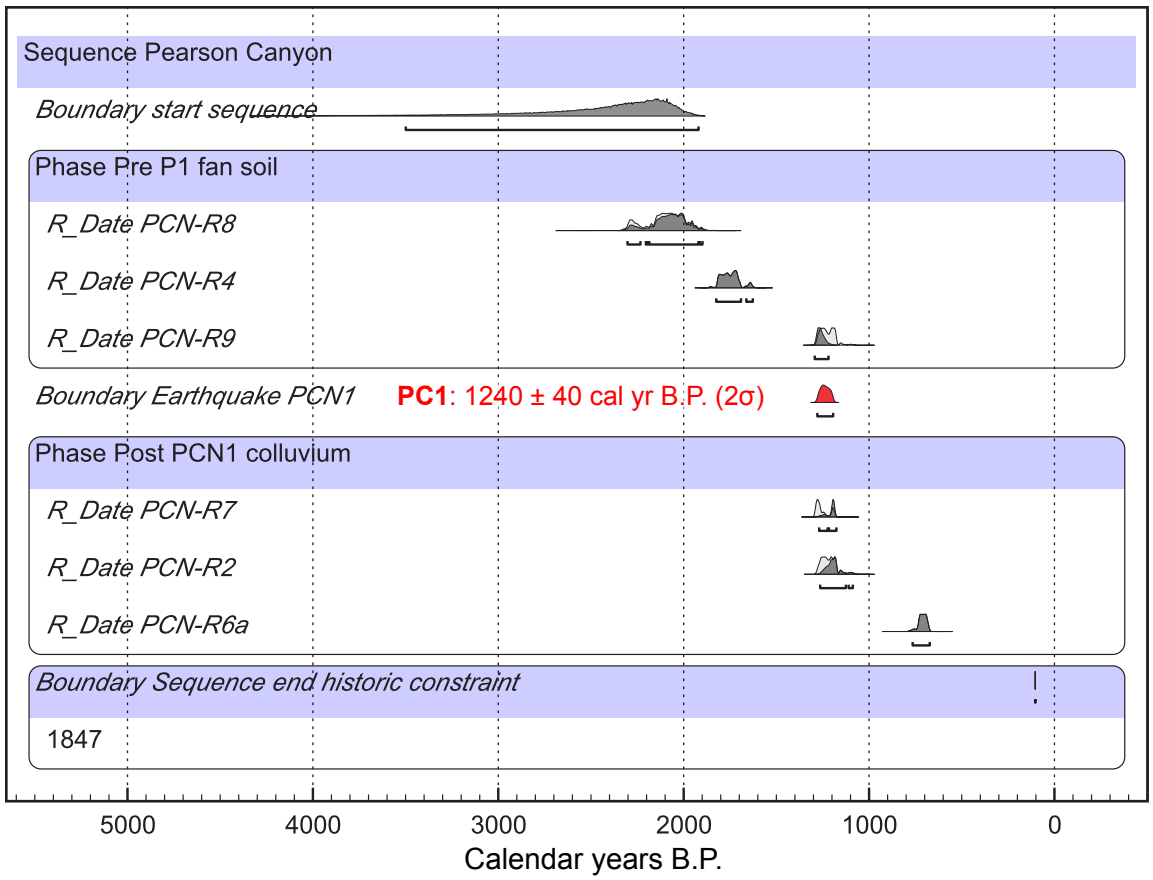

Figure 14. *OxCal model for the Pearsons Canyon site, showing stratigraphic ordering of ^{14}C ages (appendix C) and a probability density function (PDF) for the most recent earthquake (PC1). The three ages for soil unit 3A and the three ages from the post-event colluvium (unit 2) are separately included in unordered phases. Constructed using OxCal version 4.1 (Bronk Ramsey, 1995, 2001) and the IntCal09 radiocarbon calibration curve (Reimer and others, 2009). Brackets below PDFs indicate 2σ time ranges.*

offset (figure 16) and extend to within 3 km of the southern tip of the segment, where they are obscured by heavy vegetation and urban development. These scarps extend as far north as Cook Canyon (1 km south of Willard Canyon), about 2 km north of Pearsons Canyon, based on 1970s low-sun-angle photographs (flight line WF5-9, frames 145–146; Cluff and others, 1970; Bowman and others, 2009) that show a faint scarp on late(?) Holocene debris-flow deposits. However, we were unable to locate the scarp during our field reconnaissance. Considering the apparent young age of these scarps and offsets similar to the Pearsons Canyon earthquake displacement (<1 m), we interpret these scarps as the southern extent of the most recent (1.2 ka) Pearsons Canyon earthquake.

Partial Rupture of the Brigham City Segment

Paleoseismic and geomorphic data indicate that an earthquake ruptured the southernmost BCS at about 1.2 ka. This event had 0.1–0.8 m of vertical displacement at Pearsons Canyon, likely ~1–2 m of vertical offset along the southern 6–9 km

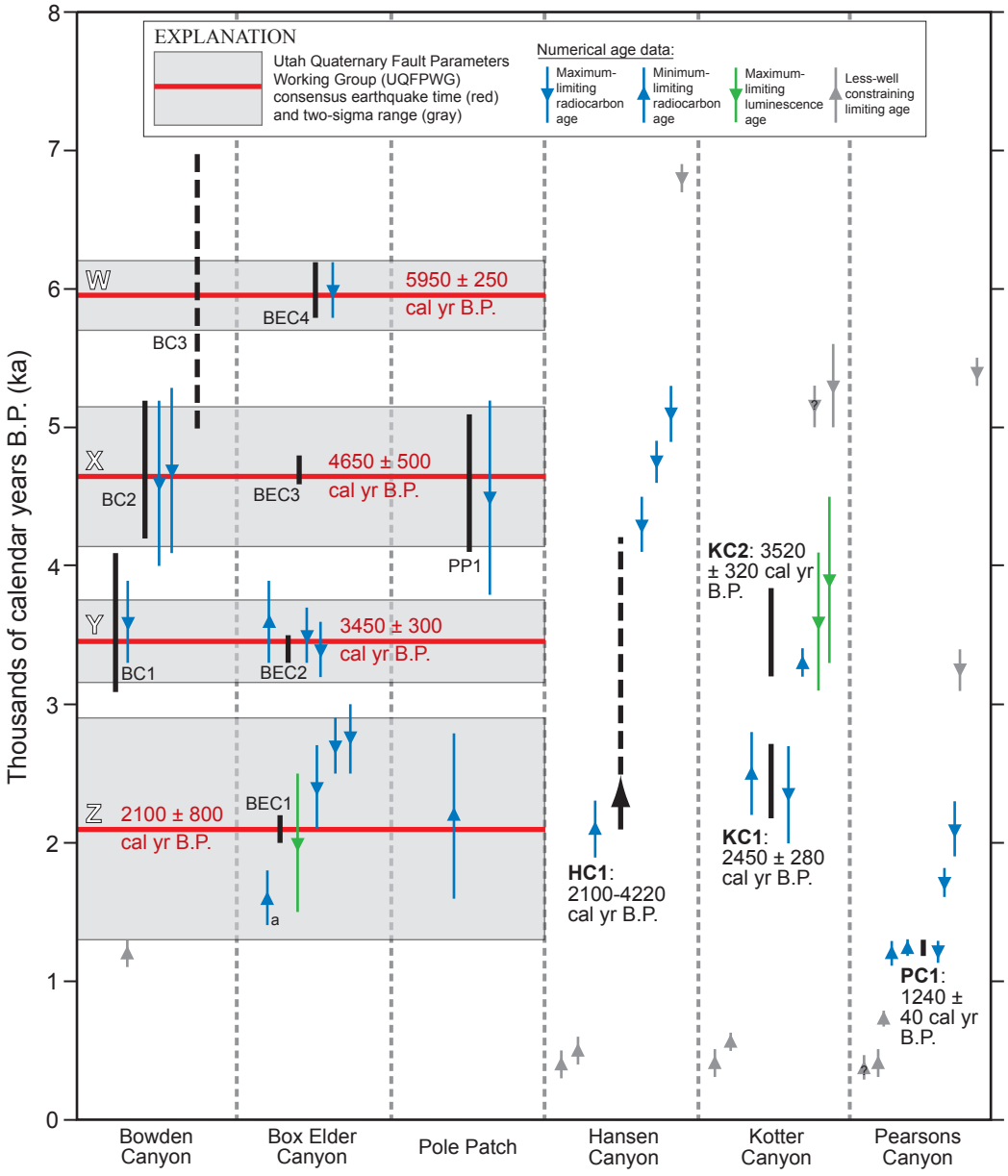

Figure 15. *Summary of BCS paleoseismic data, showing limiting ^{14}C and luminescence (OSL and TL) ages (blue and green arrows) and preferred earthquake timing (heavy black lines). Preferred times for the Hansen Canyon, Kotter Canyon, and Pearsons Canyon sites are based on this study (see text for discussion); the dashed line for Hansen Canyon indicates the poor maximum constraint for this earthquake. Preferred times for Bowden Canyon, Box Elder Canyon, and Pole Patch are based on Personius (1991a, 1991b) and McCalpin and Forman (2002). Gray boxes and red lines indicate the consensus earthquake time ranges and preferred timing of the Utah Quaternary Fault Parameters Working Group (Lund, 2005).*

of the BCS, and was not identified at the four northern BCS trench sites. Thus, an important question is whether this earthquake represents (1) the partial and independent rupture of the southern BCS or (2) the continuation of a Weber-segment rupture across the Pleasant View salient and onto the southern BCS (rupture spillover).

The Pearsons Canyon earthquake at 1.2 ka corresponds well with the timing of the second (penultimate) earthquake on the Weber segment at 1.1 ± 0.6 ka (DuRoss and others, 2009, 2011), and thus may represent the continuation of the Weber-segment penultimate earthquake rupture to the north, across the Pleasant View salient (figure 17). Paleoseismic data for the 1.1-ka Weber-segment event are from investigations at Rice Creek (0.8–1.4 ka; DuRoss and others 2009), Garner Canyon (0.6–1.5 ka; Nelson and others, 2006), and East Ogden (0.5–1.7 ka; Nelson and others, 2006), all on the northern half of the Weber segment. We suspect that the 1.1-ka earthquake also ruptured the Kaysville site on the southern half of the Weber segment based on the mapping of Swan and others (1980, 1981) and ^{14}C ages included in McCalpin and others (1994).

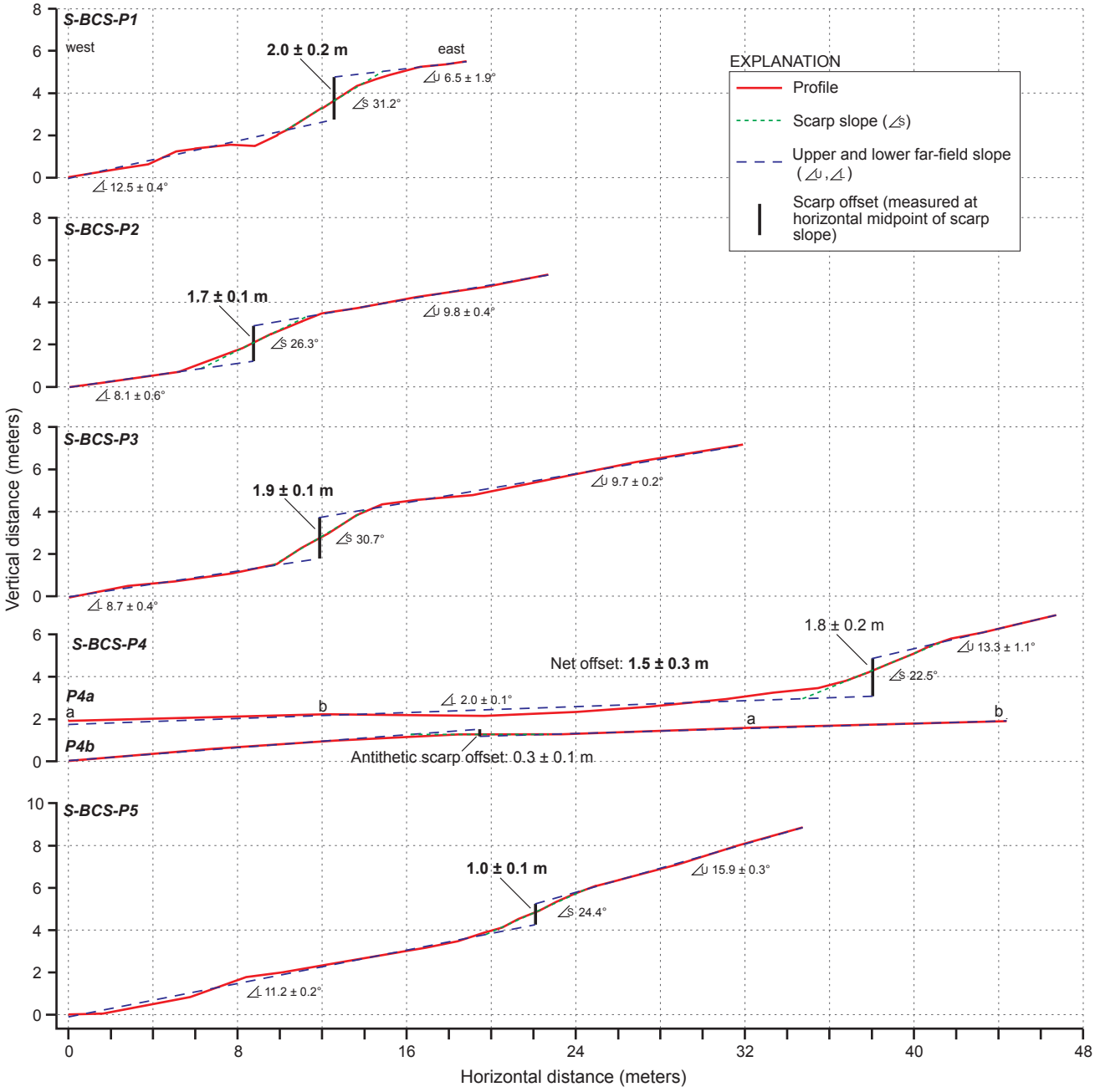

Figure 16. *Vertical surface offset from scarp profiles P1–P5 measured across late Holocene(?) alluvial-fan surfaces along the southern Brigham City segment. For profile S-BCS-P4, a and b indicate match points between profile P4a and P4b. Profile locations shown on figure 5. No vertical exaggeration.*

However, McCalpin and others (1994) did not recognize this event at Kaysville and thus, there is uncertainty regarding the southern extent of the 1.1-ka Weber-segment rupture. A younger earthquake occurred on the Weber segment at about 0.4–0.6 ka (Nelson and others, 2006; DuRoss and others, 2009), and at least two older earthquakes occurred on the segment between 2 and 5 ka (figure 17).

The extent and displacement of the 1.2-ka BCS earthquake are more consistent with spillover from the northern Weber segment, rather than an isolated partial rupture of the southern BCS. Scarps on presumed late Holocene deposits suggest that the earthquake was limited to about the southern 9 km of the BCS (south of Willard Canyon); however, a 9-km long fault rupture would only generate an earthquake of

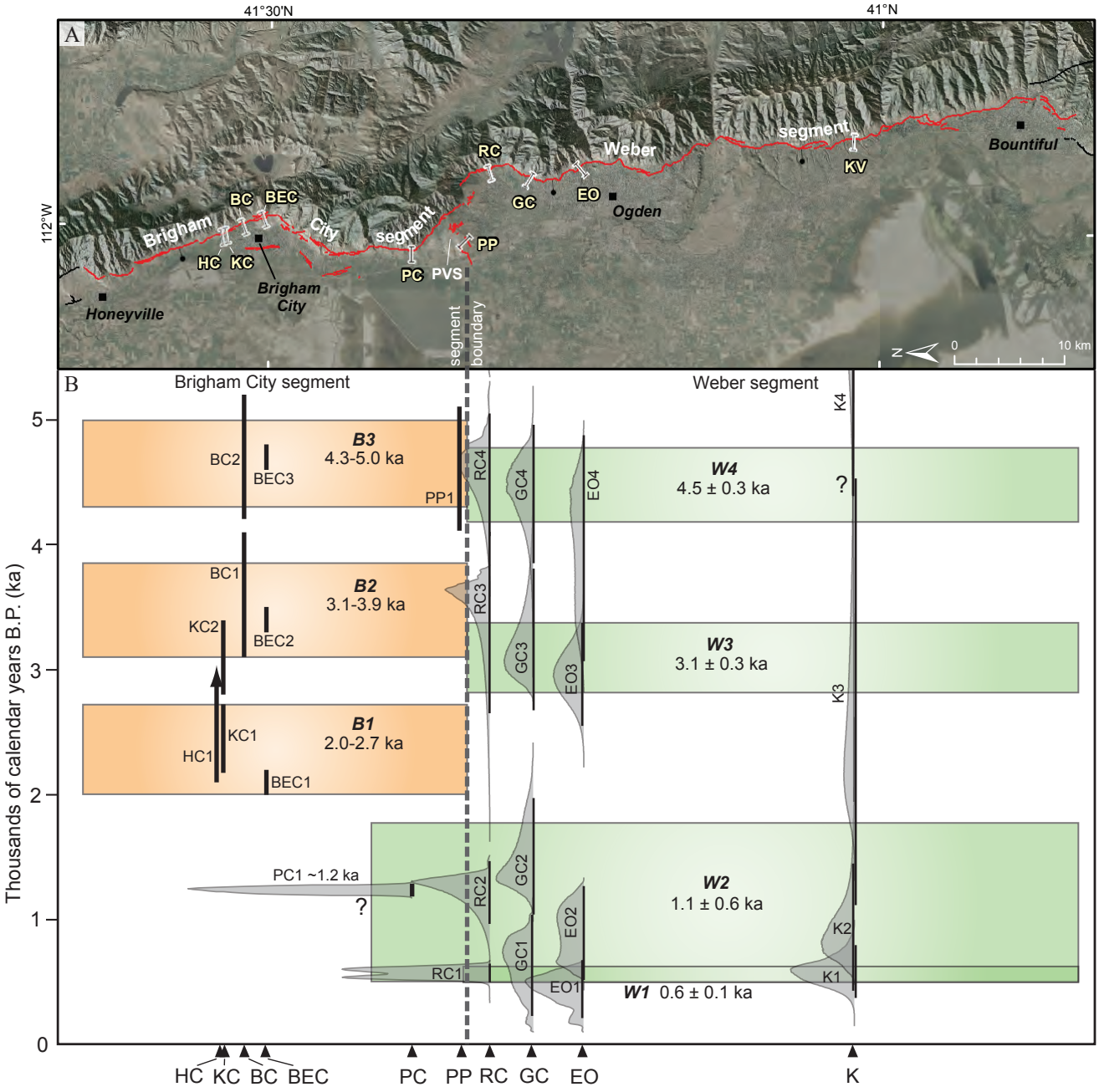

Figure 17. *Comparison of paleoseismic data for the Brigham City and Weber segments, showing (A) their surface traces and (B) mid-Holocene to present earthquake histories. For the BCS, vertical lines represent preferred earthquake time ranges per site (tables 1 and 2; arrow for HC1 reflects the event's poor maximum constraint) and orange boxes represent estimated earthquake times for BCS earthquakes B3–B1 modified from Lund (2005). Weber-segment earthquakes W4–W1, their mean times and 2σ ranges (green boxes), and time distributions (gray-shaded PDFs) are from DuRoss and others (2011). Paleoseismic site abbreviations: BC – Bowden Canyon, BEC – Box Elder Canyon, EO – East Ogden, GC – Garner Canyon, HC – Hansen Canyon, K – Kaysville, KC – Kotter Canyon, PC – Pearsons Canyon, RC – Rice Creek; PVS – Pleasant View salient. Base maps: 2006 NAIP aerial photography (USDA, 2008) and 30-m DEM (UAGRC, 2012).*

moment magnitude 6.1–6.2 (using the surface-rupture-length–magnitude regressions of Wells and Coppersmith, 1994) (plate 3), which is below the generally accepted M 6.5 surface-faulting threshold (Wells and Coppersmith, 1993) in the western U.S. Using conservative average and maximum displacements of 0.5 and 0.8 m (respectively), the earthquake likely had a surface-rupture length in excess of 20 km based on normal-fault type regressions of Wells and Coppersmith (1994). In addition, for a 1-m observed displacement, Biasi and Weldon (2006) predict a 95% likelihood that the surface rupture length is equal to or greater than about 16 km. Although it is possible that the earthquake ruptured a 17 km length of the segment from just south of Box Elder Canyon to the southern end of the BCS, Personius (1990) does not show displaced late Holocene alluvial-fan surfaces north of Willard Canyon. Thus, we consider it more likely that the 1.2-ka Brigham City earthquake represents the tail end of a considerably longer rupture originating on the Weber segment to the south.

Large displacements for the penultimate Weber-segment earthquake also support spillover rupture from the Weber segment to the BCS. Displacements for the 1.1-ka Weber segment earthquake average about 2.3 m, based on measurements of 2.6 m at East Ogden (Nelson and others, 2006), 1.0–1.3 m at Garner Canyon (Nelson and others, 2006), and 2.7–3.7 m at Rice Creek (DuRoss and others, 2009). The 1.1-ka earthquake may have also ruptured the Kaysville site, where surface faulting earthquakes have produced on average 2 m of displacement per event (based on DuRoss, 2008). Thus, it is plausible that displacement in the 1.1-ka earthquake increases northward, to a maximum of ~3.2 m at Rice Creek, 3 km from the northern end of the segment. The displacement at Garner Canyon (~1.2 m) is a poorly constrained average based on the scarp offset divided by the number of earthquakes. A northward increase in displacement and the very large displacement at the extreme northern end of the segment could reflect a northward-propagating rupture that continued through the Pleasant View salient and onto the BCS.

DISCUSSION

Faults and earthquakes in the Basin and Range Province (BRP) demonstrate the occurrence of multiple-segment and spillover ruptures. DePolo and others (1991) showed that large BRP earthquakes have complex rupture traces, with primary (large and continuous) and secondary (small and discontinuous) displacements often occurring across mapped geometric (e.g., step-over) and structural (e.g., fault-intersection) segment boundaries. Crone and others (1987) observed spillover rupture from the 1983 M7.3 Borah Peak earthquake, which led Crone and Haller (1991) to conclude that all segment boundaries must fail at some point and that persistent, but "leaky" segment boundaries may exist. Zhang and others (1999) showed that structural discontinuities (e.g., fault steps) that ruptured as part of historical BRP normal-fault rupture zones were as large as about 5 km wide, and Wesnousky (2008) demonstrated that historical normal-faulting-earthquake ruptures have crossed steps in the fault trace as wide as 7 km with 70% frequency (Wesnousky, 2008). Thus, segment boundaries do not always impede rupture, as both primary and secondary faulting may occur across them depending on factors such as the fault-trace geometry, earthquake energy, rupture propagation direction, and history of strain accumulation and release.

If the Pearsons Canyon earthquake represents the northern extension of the 1.1 ± 0.6 ka Weber-segment penultimate earthquake, then an important question is whether the Brigham City rupture occurred coseismically with the Weber segment earthquake (as primary rupture), or as triggered slip (secondary rupture), which would not contribute significantly to the Weber-segment earthquake energy release. Judging by the short length of the Brigham City rupture (6–9 km), the modest amount of displacement (0.1–0.8 m and possibly as large as 2 m based on scarp profiles), and the simple geometry and continuity of young scarps on the southern 9 km of the segment, we interpret the Pearsons Canyon earthquake as coseismic rupture associated with the 1.1-ka Weber-segment earthquake. Although the Pleasant View salient is a complex structure that has likely impeded numerous Brigham City or Weber-segment earthquake ruptures in the past, scarps on the youngest deposits at the salient form a relatively simple and continuous fault trace at the base of the range that extends north to about Willard Canyon. These scarps are only separated from the northern Weber segment by a 1.5-km left step. Thus, it is plausible that the southern 6 km (Pearsons Canyon to the end of the segment) and possibly the southern 9 km (Willard Canyon to the southern end of the segment) of the BCS ruptured as part of the 1.1-ka Weber-segment earthquake (figure 17). North of Willard Canyon, the fault trace is considerably more complex and the ages and deformation of displaced deposits do not indicate late Holocene faulting.

Our analysis of earthquakes on the BCS is the first to provide compelling paleoseismic evidence of a WFZ segment-boundary failure. Earlier WFZ studies either recognized geomorphic evidence in support of rupture spillover, or considered multi-segment ruptures possible based on earthquake-timing data. For example, fault-scarp offset and relative-timing data suggest rupture across the Brigham City–Collinston (Personius, 1990; Hylland, 2007b) and Levan–Fayette (Hylland, 2007a; Hylland and Machette, 2008) segment boundaries. DuRoss and others (2008) discussed the potential for coseismic rupture of the Provo and northern Nephi segments, but could not rule out single-segment ruptures because of broadly constrained earthquake times. Finally, Chang and Smith (2002) included both single-segment and multi-segment rupture scenarios in their hazard analysis of the central WFZ. Thus, our results are significant in that they offer strong earthquake timing and displacement evidence of rupture across a WFZ segment boundary.

The coseismic rupture of the Weber segment and southernmost BCS has important implications for earthquake hazards. Adding 9 km of BCS rupture to a Weber segment earthquake would increase its rupture length from 56 to 65 km, raise the moment magnitude from 7.1 to 7.2 (based on the all-fault-type surface-rupture-length–M_W regression of Wells and Coppersmith, 1994) (table 3), and increase the earthquake energy release (seismic moment, M_0) by 16% (from 9.0 x 10^{26} to 1.0 x 10^{27} dyne-cm; table 3). In addition, the spillover rupture reduces the (straight-line) length of the BCS that has not ruptured in ~2 kyr from 36 km to 28 km (table 3). However, we are uncertain whether the partial rupture has increased or decreased the likelihood of a surface-faulting earthquake on the northern BCS.

CONCLUSIONS

Our paleoseismic investigations at Hansen Canyon and Kotter Canyon clarify the timing and displacement of late Holocene earthquakes on the BCS, and importantly, confirm that the youngest earthquake on the north-central BCS occurred before 2 ka. We constrained the timing of the youngest earthquakes at these sites to 2.1–4.2 ka (Hansen Canyon) and 2.5 ± 0.3 ka (Kotter Canyon), consistent with the mean age of 2.1 ka for the youngest earthquake identified at Box Elder Canyon. These data are strong evidence of a long elapsed time (about 2.1–2.8 ka) since the most recent earthquake on most of the BCS, which significantly exceeds the 1.3-kyr mean recurrence interval for the BCS. This long elapsed time demonstrates that either (1) the BCS has the highest time-dependent earthquake probability of the central WFZ (e.g., Wong and others, 2002), or (2) that the recurrence of earthquakes on the BCS is poorly understood and possibly aperiodic, conceivably as a result of strain release on Holocene faults to the east or west (e.g., the West Cache fault zone).

Paleoseismic data from Pearsons Canyon, on the previously unstudied southern BCS, indicate that a post-2 ka earthquake ruptured this part of the segment. The youngest Pearsons Canyon earthquake (PC1) is well constrained to 1.2 ± 0.04 ka, consistent with our observation of continuous, youthful scarps on the southern 9 km of the BCS having 1–2 m of late Holocene(?) surface offset. The timing of PC1 and the surface-offset data are compelling evidence of spillover rupture from the Weber segment to the southern BCS (across the Pleasant View salient), likely in the penultimate Weber-segment earthquake at 1.1 ± 0.6 ka. Moderate displacements but a limited (9-km) extent of the 1.2-ka BCS rupture, large displacements at the northern end of the Weber segment in the 1.1-ka penultimate earthquake, and the simple geometry of the Holocene fault trace across the Pleasant View salient also support a Weber to Brigham City segment spillover rupture. Implications of surface faulting across the Weber-Brigham City segment boundary include (1) an increased rupture length and energy release for the Weber-segment penultimate earthquake, (2) a revised length of the BCS that has not ruptured since 2 ka (with time-dependent probability implications), and (3) strong evidence of at least one segment-boundary failure and multi-segment rupture on the central WFZ.

ACKNOWLEDGMENTS

This paleoseismic study was supported by the U.S. Geological Survey National Earthquake Hazards Reduction Program (award no. 08HQGR0082) and the Utah Geological Survey. Ashley Elliot and Keith Beisner assisted with fieldwork. We greatly appreciate the interest and cooperation of the landowners of each of our study sites and thank them for granting access to their property. Specifically, we thank David Tea for access to the Hansen Canyon site, Bliss Law for providing access to the Kotter Canyon site, and William Marsh and family for granting access to the Pearsons Canyon site. Reviews by Steve Bowman, Mike Hylland, and Bill Lund (UGS), and Susan Olig (URS Corporation) strengthened this report.

REFERENCES

Aitken, M.J., 1994, Optical dating—a non-specialist review: Quaternary Geochronology (Quaternary Science Reviews), v. 13, p. 503–508.

Biasi, G.P., and Weldon, R.J., 2006, Estimating surface rupture length and magnitude of paleoearthquakes from point measurements of rupture displacement: Bulletin of the Seismological Society of America, v. 96, no. 5, p. 1612–1623.

Birkeland, P.W., Machette, M.N., and Haller, K.M., 1991, Soils as a tool for applied Quaternary geology: Utah Geological and Mineral Survey Miscellaneous Publication 91-3, 63 p.

Black, B.D., Hecker, S., Hylland, M.D., Christenson, G.E., and McDonald, G.N., 2003, Quaternary fault and fold database and map of Utah: Utah Geological Survey Map 193DM, scale 1:50,000, CD.

Bowman, S.D., Beisner, K., and Unger, C., 2009, Compilation of 1970s Woodward-Lundgren & Associates Wasatch fault investigation reports and oblique aerial photography, Wasatch Front and Cache Valley, Utah and Idaho: Utah Geological Survey Open-File Report 548, 3 p., 6 plates, 9 DVDs.

Bronk Ramsey, C., 1995, Radiocarbon calibration and analysis of stratigraphy—the OxCal program: Radiocarbon, v. 37, no. 2, p. 425–430.

Bronk Ramsey, C., 2001, Development of the radiocarbon program OxCal: Radiocarbon, v. 43, no. 2a, p. 355–363.

Bronk Ramsey, C., 2008, Depositional models for chronological records: Quaternary Science Reviews, v. 27, no. 1-2, p. 42–60.

Chang, W.L., and Smith, R.B., 2002, Integrated seismic-hazard analysis of the Wasatch Front, Utah: Bulletin of the Seismological Society of America, v. 92, no. 5, p. 1904–1922.

Chang, W.L., Smith, R.B., Meertens, C.M., and Harris, R.B., 2006, Contemporary deformation of the Wasatch fault, Utah, from GPS measurements with implications for interseismic fault behavior and earthquake hazard—observations and kinematic analysis: Journal of Geophysical Research, v. 111, 19 p.

Cluff, L.S., Brogan, G.E., and Glass, C.E., 1970, Wasatch fault, northern portion—earthquake fault investigation and evaluation, a guide to land-use planning: Oakland, California, Woodward-Clyde and Associates, unpublished consultant report for the Utah Geological and Mineralogical Survey, variously paginated.

Crone, A.J., and Haller, K.M., 1991, Segmentation and the coseismic behavior of Basin and Range normal faults—examples from east-central Idaho and southwestern Montana, U.S.A.: Journal of Structural Geology, v. 13, no. 2, p. 151–164.

Crone, A.J., Machette, M.N., Bonilla, M.G., Lienkaemper, J.J., Pierce, K.L., Scott, W.E., and Bucknam, R.C., 1987, Surface faulting accompanying the Borah Peak earthquake and segmentation of the Lost River fault, central Idaho: Bulletin of the Seismological Society of America, v. 77, p. 739–770.

dePolo, C.M., Clark, D.G., Slemmons, D.B., and Ramelli, A.R., 1991, Historical surface faulting in the Basin and Range Province, western North America—implications for fault segmentation: Journal of Structural Geology, v. 13, no. 2, p. 123–136.

DuRoss, C.B., 2008, Holocene vertical displacement on the central segments of the Wasatch fault zone, Utah: Bulletin of the Seismological Society of America, v. 98, no. 6, p. 2918-2933.

DuRoss, C.B., McDonald, G.N., and Lund, W.R., 2008, Paleoseismic investigation of the northern strand of the Nephi segment of the Wasatch fault zone at Santaquin, Utah—Paleoseismology of Utah, Volume 17: Utah Geological Survey Special Study 124, 33 p., 1 plate, CD.

DuRoss, C.B., Personius, S.F., Crone, A.J., McDonald, G.N., and Lidke, D.J., 2009, Paleoseismic investigation of the northern Weber segment of the Wasatch fault zone at the Rice Creek trench site, North Ogden, Utah—Paleoseismology of Utah, Volume 18: Utah Geological Survey Special Study 130, 37 p., 2 plates, CD.

DuRoss, C.B., Personius, S.F., Crone, A.J., Olig, S.S., and Lund, W.R., 2011, Integration of paleoseismic data from multiple sites to develop an objective earthquake chronology—application to the Weber segment of the Wasatch fault zone, Utah: Bulletin of the Seismological Society of America, v. 101, no. 6, p. 2765–2781.

Forman, S.L., Nelson, A.R., and McCalpin, J.P., 1991, Thermoluminescence dating of fault-scarp-derived colluvium—deciphering the timing of earthquakes on the Weber segment of the Wasatch fault zone, north-central Utah: Journal of Geophysical Research, v. 96, no. B1, p. 595–605.

Friedrich, A.M., Wernicke, B.P., Niemi, N.A., Bennett, R.A., and Davis, J.L., 2003, Comparison of geodetic and geologic data from the Wasatch region, Utah, and implications for the spectral character of Earth deformation at periods of 10 to 10 million years: Journal of Geophysical Research, v. 108, no. B4, p. 7-1–7-23, doi:10.1029/2001JB000682.

Gavin, D.G., 2001, Estimation of inbuilt age in radiocarbon ages of soil charcoal for fire history studies: Radiocarbon, v. 43, no. 1, p. 27–44.

Godsey, H.S., Currey, D.R., and Chan, M.A., 2005, New evidence for an extended occupation of the Provo shoreline and implications for regional climate change, Pleistocene Lake Bonneville, Utah, USA: Quaternary Research, v. 63, no. 2, p. 212–223.

Hanks, T.C., and Kanamori, H., 1979, A moment magnitude scale: Journal of Geophysical Research, v. 84, no. B5, p. 2348–2350.

Harmon, M.E., Franklin, J.F., Swanson, F.J., Sollins, P., Gregory, S.V., Lattin, J.D., Anderson, N.H., Cline, S.P., Aumen, N.G., Sedell, J.R., Lienkaemper, G.W., Cromack, K., Jr., and Cummins, K.W., 1986, Ecology of coarse woody debris in temperate ecosystems: Advances in Ecological Research, v. 15, p. 133–302.

Huntley, D.J., Godfrey-Smith, D.I., and Thewalt, M.L.W., 1985, Optical dating of sediments: Nature, v. 313, p. 105–107.

Hylland, M.D., 2007a, Spatial and temporal patterns of surface faulting on the Levan and Fayette segments of the Wasatch fault zone, central Utah, from surficial geologic mapping and scarp-profile data, *in* Willis, G.C., Hylland, M.D., Clark, D.L., and Chidsey, T.C., Jr., editors, Central Utah—diverse geology of a dynamic landscape: Utah Geological Association Publication 36, p. 255–271.

Hylland, M.D., 2007b, Surficial-geologic reconnaissance and scarp profiling on the Collinston and Clarkston Mountain segments of the Wasatch fault zone, Box Elder County, Utah—paleoseismic inferences, implications for adjacent segments, and issues for diffusion-equation scarp-age modeling—Paleoseismology of Utah, Volume 15: Utah Geological Survey Special Study 121, 18 p., CD.

Hylland, M.D., and Machette, M.N., 2008, Surficial geologic map of the Levan and Fayette segments of the Wasatch fault zone, Juab and Sanpete Counties, Utah: Utah Geological Survey Map 229, 37 p. pamphlet, 1 plate, scale 1:50,000.

Lienkaemper, J.J., and Bronk Ramsey, C., 2009, OxCal—versatile tool for developing paleoearthquake chronologies—a primer: Seismological Research Letters, v. 80, no. 3, p. 431–434.

Lund, W.R., 2005, Consensus preferred recurrence-interval and

vertical slip-rate estimates—review of Utah paleoseismic-trenching data by the Utah Quaternary Fault Parameters Working Group: Utah Geological Survey Bulletin 134, variously paginated, CD.

Machette, M.N., Crone, A.J., Personius, S.F., Mahan, S.A., Dart, R.L., Lidke, D.J., and Olig, S.S., 2007, Paleoseismology of the Nephi segment of the Wasatch fault zone, Juab County, Utah—preliminary results from two large exploratory trenches at Willow Creek: U.S. Geological Survey Scientific Investigations Map SI-2966, 2 plates.

Machette, M.N., Personius, S.F., and Nelson, A.R., 1992, Paleoseismology of the Wasatch fault zone—a summary of recent investigations, interpretations, and conclusions, *in* Gori, P.L., and Hays, W.W., editors, Assessment of regional earthquake hazards and risk along the Wasatch Front, Utah: U.S. Geological Survey Professional Paper 1500-A, p. A1–A71.

Matthews, M.H., 1979, Soil sample analysis of 5MT2148—Dominguez Ruin, Dolores, Colorado, *in* Reed, A.D., editor, The Dominguez Ruin—a McElmo Phase pueblo in southwestern Colorado: Bureau of Land Management Cultural Resource Series, v. 7, variously paginated.

McCalpin, J.P., 1996, Paleoseismology in extensional tectonic environments, *in* McCalpin, J.P., editor, Paleoseismology: San Diego, Academic Press, p. 85–146.

McCalpin, J.P., 2002, Post-Bonneville paleoearthquake chronology of the Salt Lake City segment, Wasatch fault zone, from the 1999 "megatrench" site—Paleoseismology of Utah, Volume 10: Utah Geological Survey Miscellaneous Publication 02-7, 37 p.

McCalpin, J.P., and Forman, S.L., 2002, Post-Provo earthquake chronology of the Brigham City segment, Wasatch fault zone, Utah—Paleoseismology of Utah, Volume 11: Utah Geological Survey Miscellaneous Publication 02-9, 46 p.

McCalpin, J.P., Forman, S.L., and Lowe, M., 1994, Reevaluation of Holocene faulting at the Kaysville site, Weber segment of the Wasatch fault zone, Utah: Tectonics, v. 13, no. 1, p. 1–16.

McCalpin, J.P., and Nishenko, S.P., 1996, Holocene paleoseismicity, temporal clustering, and probabilities of future large (M>7) earthquakes on the Wasatch fault zone: Journal of Geophysical Research, v. 101, no. B3, p. 6233–6253.

National Aeronautics & Space Administration, 2006, Visible Earth—a catalog of NASA images and animations of our home planet: Online, <http://visibleearth.nasa.gov/>, accessed July 2006.

Nelson, A.R., Lowe, M., Personius, S., Bradley, L.A., Forman, S.L., Klauk, R., and Garr, J., 2006, Holocene earthquake history of the northern Weber segment of the Wasatch fault zone, Utah—Paleoseismology of Utah, Volume 13: Utah Geological Survey Miscellaneous Publication 05-8, 39 p., 2 plates, CD.

Nelson, A.R., and Personius, S.F., 1993, Surficial geologic map of the Weber segment, Wasatch fault zone, Weber and Davis Counties, Utah: U.S. Geological Survey Miscellaneous Investigations Series Map I-2199, 22 p. pamphlet, scale 1:50,000.

Olig, S.S., McDonald, G., Black, B.D., DuRoss, C.B., Lund, W.R., Hylland, M., Simon, D.B., Giraud, R.E., and Christenson, G.E., 2011, Extending the paleoseismic record of the Provo segment of the Wasatch fault zone, Utah: Final Technical Report to the U.S. Geological Survey, variously paginated.

Oviatt, C.G., 1997, Lake Bonneville fluctuations and global climate change: Geology, v. 25, p. 155–158.

Oviatt, C.G., Currey, D.R., and Miller, D.M., 1990, Age and paleoclimatic significance of the Stansbury shoreline of Lake Bonneville, northeastern Great Basin: Quaternary Research, v. 33, p. 291–305.

Oviatt, C.G., Currey, D.R., and Sack, D., 1992, Radiocarbon chronology of Lake Bonneville, eastern Great Basin, USA: Palaeogeography, Palaeoclimatology, Palaeoecology, v. 99, p. 225–241.

Personius, S.F., 1990, Surficial geologic map of the Brigham City segment and adjacent parts of the Weber and Collinston segments, Wasatch fault zone, Box Elder and Weber Counties, Utah: U.S. Geological Survey Miscellaneous Investigations Series Map I-1979, scale 1:50,000.

Personius, S.F., 1991a, Paleoseismic analysis of the Wasatch fault zone at the Brigham City trench site, Brigham City, Utah—Paleoseismology of Utah, Volume 2: Utah Geological and Mineral Survey Special Study 76, p. 1–18.

Personius, S. F., 1991b, Paleoseismic analysis of the Wasatch fault zone at the Pole Patch trench site, Pleasant View, Utah – Paleoseismology of Utah, Volume 2: Utah Geological and Mineral Survey Special Study 76, p. 19–39.

Petersen, M.D., Frankel, A.D., Harmsen, S.C., Mueller, C.S., Haller, K.M., Wheeler, R.L., Wesson, R.L., Zeng, Y., Boyd, O.S., Perkins, D.M., Luco, N., Field, E.H., Wills, C.J., and Rukstales, K.S., 2008, Documentation for the 2008 update of the United States National Seismic Hazard Maps: U.S. Geological Survey Open-File Report 2008-1128, 61 p.

Prescott, J.R., and Hutton, J.T., 1994, Cosmic ray contributions to dose rates for luminescence and ESR dating: Radiation Measurements, v. 23, p. 497–500.

Puseman, K., and Cummings, L.S., 2005, Separation and identification of charcoal and organics from bulk sediment samples for improved radiocarbon dating and stratigraphic correlations, *in* Lund, W.R., editor, Western States Seismic Policy Council Proceedings Volume of the Basin and Range Province Seismic Hazards Summit II: Utah Geological Survey Miscellaneous Publication 05-2, 10 p., CD.

Reimer, P.J., Baillie, M.G.L., Bard, E., Bayliss, A., Beck, J.W., Blackwell, P.G., Bronk Ramsey, C., Buck, C.E., Burr, G.S., Edwards, R.L., Friedrich, M., Grootes, P.M., Guilderson, T.P., Hajdas, I., Heaton, T.J., Hogg, A.G., Hughen,

K.A., Kaiser, K.F., Kromer, B., McCormac, F.G., Manning, S.W., Reimer, R.W., Richards, D.A., Southon, J.R., Talamo, S., Turney, C.S. M., van der Plicht, J., and Weyhenmeyer, C.E., 2009, IntCal09 and Marine09 radiocarbon age calibration curves, 0–50,000 years cal BP: Radiocarbon, v. 51, no. 4, p. 1111–1150.

Schwartz, D.P., and Coppersmith, K.J., 1984, Fault behavior and characteristic earthquakes—examples from the Wasatch and San Andreas fault zones: Journal of Geophysical Research, v. 89, p. 5681–5698.

Swan, F.H., III, Schwartz, D.P., and Cluff, L.S., 1980, Recurrence of moderate to large magnitude earthquakes produced by surface faulting on the Wasatch fault zone, Utah: Bulletin of the Seismological Society of America, v. 70, p. 1431–1462.

Swan, F.H., III, Schwartz, D.P., Hanson, K.L., Knuepfer, P.L., and Cluff, L.S., 1981, Study of earthquake recurrence intervals on the Wasatch fault at the Kaysville site, Utah: U.S. Geological Survey Open-File Report 81-228, 30 p.

U.S. Department of Agriculture, 1993, Soil Survey Manual: Online, <http://soils.usda.gov/technical/manual/>, accessed April 2009.

U.S. Department of Agriculture, 2008, Aerial photography field office—National Agriculture Imagery Program: Online, <http://165.221.201.14/ NAIP.html>, accessed August 2008.

Utah Automated Geographic Reference Center, 2012, Utah GIS Portal: Online, <http://gis.utah.gov/agrc>, accessed January 2012.

Wells, D.L., and Coppersmith, K.J., 1993, Likelihood of surface rupture as a function of magnitude: Seismological Research Letters, v. 64, no. 1, p. 54.

Wells, D.L., and Coppersmith, K.J., 1994, New empirical relationships among magnitude, rupture length, rupture width, rupture area, and surface displacement: Bulletin of the Seismological Society of America, v. 84, no. 4, p. 974–1002.

Wesnousky, S.G., 2008, Displacement of geometrical characteristics of earthquake surface ruptures – issues and implications for seismic-hazard analysis and the process of earthquake rupture: Bulletin of the Seismological Society of America, v. 98, no. 4, p. 1609–1632.

Wong, I., Silva, W., Olig, S., Thomas, P., Wright, D., Ashland, F., Gregor, N., Pechmann, J., Dober, M., Christenson, G., and Gerth, R., 2002, Earthquake scenario and probabilistic ground shaking maps for the Salt Lake City, Utah, metropolitan area: Utah Geological Survey Miscellaneous Publication 02-5, 48 p.

Zhang, P., Mao, F., and Slemmons, D.B., 1999, Rupture terminations and size of segment boundaries from historical earthquake ruptures in the Basin and Range Province: Tectonophysics, v. 308, no. 1-2, p. 37–52.

APPENDIX A

DESCRIPTION OF STRATIGRAPHIC UNITS IN TRENCHES AT THE HANSEN CANYON, KOTTER CANYON, AND PEARSONS CANYON SITES

DESCRIPTION OF STRATIGRAPHIC UNITS IN TRENCHES AT THE HANSEN CANYON, KOTTER CANYON, AND PEARSONS CANYON SITES

Unit; location (m)[1]	Matrix texture[2]	% matrix/ gravel[3]	Clasts		Clast or matrix support	Sorting	Bedding	Color[4] dry (moist)	Consistence[5]		Lower boundary[6]	Soil development[7]	Genesis
			% 0.2–1cm/ 1–3cm/ >3cm	Largest/ avg size (cm)					Dry	Wet			
Hansen Canyon													
1; 16.5, 7.9	silty loam	40/60	40/40/20	80/20-40	clast and matrix	poor	very crudely bedded to massive; local boulder lenses	7.5YR4/2 (7.5YR3/2)	lo-so	ss/ps	a-c/s-w	A horizon (0-5 cm depth)	pebble-rich debris flow
2; 15.5, 7.7	loam - sandy loam	25/75	20/30/50	130-140/ 50-70	clast and matrix	very poor	massive; slope-parallel clasts	7.5YR4/4 (7.5YR3/3)	so	so-ss/ps	a/i (tect)	none	fault-scarp colluvium
3A; 19.6, 7.3	loam - silty loam	50/50	25/25/50	200-240/ 50-80	clast	poor	massive	10YR5/3 (10YR4/4)	so	ss/ps-p	c/s	A horizon; ubiquitous organic matter	A horizon on unit 3
3; 21.1, 6.9	silty loam	30/70	10/45/45	80-100/ 30-60	clast and matrix	poor	very crudely bedded to massive; boulder lenses in footwall	10YR7/6 (10YR 5/8)	so-sh	ss/p	c/s	none, but carbonate rich matrix	cobble-rich debris flow
4; 21.0, 6.3	silty loam	50/50	30/30/40	150-200/ 50-70	matrix	poor	very crudely bedded to massive	10YR7/6 (10YR 5/6)	so-sh	so-ss/ ps-p	ne	none, but carbonate rich matrix	pebble-rich debris flow
Kotter Canyon													
1; 23.9, 11.0	silty loam	60/40	30/35/30	15/3	clast	moderate	massive; slope-parallel clasts	10YR5/4 (10YR4/3)	sh	ss/ps	a-c/s-w	modern A horizon (0-10 cm depth); Bw (10-25 cm)	organic-rich debris flow
2; 18.8, 12.4	loam	40/60	20/20/60	60/5-15	clast and matrix	poor	massive; crude cobble stratification	10YR5/4 (10YR4/4)	sh	ns-ss/ps	g/s	weak A horizon	fault-scarp colluvium
3; 18.7, 12.1	sandy loam	40/60	25/25/50	35/5-8	clast	poor	massive; slope-parallel clasts	7.5YR6/6 (7.5YR5/6)	so	ns/po	c/s	stripped Bw horizon	fault-scarp colluvium
2-3; 24.7, 10.1	sandy loam	40/60	30/30/40	20/4-8	clast	poor	massive	7.5YR6/6 (7.5YR5/6)	so	ns/po	c/s	weak A horizon	fault-scarp colluvium
4a-1; 30.8, 8.2	sandy loam	30/70	25/25/50	30/4-10	clast	poor	massive	10YR6/4 (10YR5/4)	so	ss/ps	a/s	A horizon near west end of trench	debris flow
4b-1; 29.0, 8.5	fine to coarse sand	20/80	30/30/40	8/2-4	clast	moderate-well	well stratified; weak cross bedding	10YR8/4 (10YR6/6)	so	ns/po	a/s	none	stream gravels (openwork)

Unit[1]	Matrix texture[2]	% matrix/ gravel[3]	Clasts		Clast or matrix support	Sorting	Bedding	Color[4] dry (moist)	Consistence[5]		Lower bound[6]	Soil development[7]	Genesis
			% 0.2–1cm/ 1–3cm/ >3cm	Largest/ avg size (cm)					Dry	Wet			
4a-2; 21.6, 10.5	sandy loam	30/70	35/35/30	30/4	clast	moderate	weakly stratified	10YR7/4 (10YR6/4)	so	ns/ss	c/s	weak A horizon	debris flow
4b-2; 21.7, 10.0	sandy loam	30/70	40/30/30	13/1-2	clast	moderate	massive	10YR7/4 (10YR6/6)	so	ns/ss	c/s	none	debris flow
4c; 21.9, 9.5	sandy loam	20/80	40/30/30	25/2-4	clast	poor	massive	10YR7/4 (10YR6/6)	so	ns/po	c/s	none	debris flow; local stream deposits in footwall
4d; 17.3, 11.7	sandy loam	30/70	40/40/20	60/2-4	clast	moderate	massive	10YR7/4 (10YR6/6)	so	ns/po	ne	none	debris flow
Pearsons Canyon													
1; 34.5, 3.1	sandy loam	40/60	40/30/30	13/2-4	clast and matrix	moderate	massive; some recycled Bonneville gravels	10YR4/3 (10YR3/2)	sh	so/ps	a/s	A horizon; ubiquitous organic matter in matrix	debris flow, post dates and partly buries antithetic scarp
2; 11.4, 7.6	loam	50/50	40/40/20	25/2-10	matrix	poor	massive, intermittent stoneline at base, some recycled Bonneville gravels	10YR4/4 (10YR2/2)	sh	ss/ps	a/s	A horizon; ubiquitous organic matter in matrix	fault-scarp colluvium
3a; 29.0, 3.5	loamy sand	40/60	35/30/35	25/2-5	clast	poor	very crudely bedded, some recycled Bonneville gravels	10YR5/6 (10YR4/4)	so	so/po	c/s	A horizon	debris flow, fan
3b; 14.5, 6.4	loamy sand	35/65	35/30/35	30/5-12	clast	poor	very crudely bedded, some recycled Bonneville gravels	10YR5/6 (10YR4/4)	lo	so/po	c/s	A horizon	debris flow, fan
3c; 14.7, 6.1	loamy sand	40/60	35/30/35	26/4-12	clast	poor	very crudely bedded, some recycled Bonneville gravels	10YR5/6 (10YR3/4)	lo	so/po	c/s	A horizon in footwall	debris flow, fan
3d; 7.3 8.5	sand	30/70	20/40/40	35/3-10	clast	poor	crudely bedded with lenses of sandy pebble gravel	10YR6/4 (10YR4/4)	lo	so/po	ne	none	mixed debris-flow and stream deposit

[1] Units and locations (horizontal and vertical meters) correspond with plates 1-3.

[2] Texture terms follow the U.S. Department of Agriculture (1993) classification system. Textural information may not be representative of entire unit due to vertical and horizontal heterogeneity in units.

[3] Percentages of clast-size fractions (based on area) are field estimates. We used a #10 (2 mm) sieve to separate matrix from gravel.

[4] Munsell color of matrix.

[5] Consistence from Birkeland and others (1991). Dry consistence: lo – loose (noncoherent), so – soft (weakly coherent), sh – slightly hard, h – hard. Wet consistence includes stickiness (so – nonsticky, ss – slightly sticky, s – sticky) and plasticity (po – nonplastic, ps – slightly plastic, p – plastic).

[6] Lower boundary modified from Birkeland and others (1991). Distinctness: a – abrupt (1mm-2.5 cm), c – clear (2.5-6 cm), g – gradual (6-12.5 cm), i - tectonic (faulted). Topography: s – smooth, w – wavy, i – irregular. ne, base of unit not exposed.

[7] Description of soil development

APPENDIX B

EXAMINATION OF BULK SOIL FOR RADIOCARBON DATABLE MATERIAL FROM THE BRIGHAM CITY SEGMENT OF THE WASATCH FAULT, UTAH

By

Kathryn Puseman

Paleo Research Institute
Golden, Colorado

Paleo Research Institute Technical Report 08-72
December 2008

INTRODUCTION

A total of 25 bulk soil samples from the three trench sites in the Brigham City segment of the Wasatch Fault zone, Utah, were floated to recover organic fragments suitable for radiocarbon analysis. Botanic components and detrital charcoal were identified, and potentially radiocarbon datable material was separated. The Hansen Canyon, Kotter Canyon, and Pearsons Canyon trench sites lie below the highest Lake Bonneville shoreline. Dating of material from the fault zones will be used to provide time limits for single surface-faulting earthquakes at the Hansen and Pearson sites, as well as two paleoevents at the Kotter site. Samples for AMS radiocarbon dating will be submitted to Woods Hole Institute.

METHODS

Flotation and Identification

The bulk samples were floated using a modification of the procedures outlined by Matthews (1979). Each sample was added to approximately 3 gallons of water. The sample was stirred until a strong vortex formed, which was allowed to slow before pouring the light fraction through a 150 micron mesh sieve. Additional water was added and the process repeated until all visible macrofloral material was removed from the sample (a minimum of five times). The material that remained in the bottom (heavy fraction) was poured through a 0.5-mm mesh screen. The floated portions were allowed to dry.

The light fractions were weighed, then passed through a series of graduated screens (US Standard Sieves with 4-mm, 2-mm, 1-mm, 0.5-mm and 0.25-mm openings to separate charcoal debris and to initially sort the remains. The contents of each screen were then examined. Charcoal pieces larger than 1-mm in diameter were broken to expose a fresh cross section and examined under a binocular microscope at a magnification of 70x. The remaining light fraction in the 4-mm, 2-mm, 1-mm, 0.5-mm, and 0.25-mm sieves was scanned under a binocular stereo microscope at a magnification of 10x, with some identifications requiring magnifications of up to 70x. The material that passed through the 0.25-mm screen was not examined. The coarse or heavy fractions also were screened and examined for the presence of botanic remains. Remains from both the light and heavy fractions were recorded as charred and/or uncharred, whole and/or fragments. Individual detrital charcoal/wood samples also were broken to expose a fresh cross-section and examined under a binocular microscope at a magnification of 70x.

Macrofloral remains, including charcoal, were identified using manuals (Core, et al. 1976; Martin and Barkley 1961; Panshin and Zeeuw 1980; Petrides and Petrides 1992) and by comparison with modern and archaeological references. The term "seed" is used to represent seeds, achenes, caryopses, and other disseminules. Because charcoal and possibly other botanic remains were to be sent for radiocarbon dating, clean laboratory conditions were used during flotation and identification to avoid contamination. All instruments were washed between samples, and samples were protected from contact with modern charcoal.

DISCUSSION

The Hansen Canyon and Kotter Canyon trench sites are located about one mile north of Brigham City, Utah, at the western base of the Wasatch Range. These sites are situated at an elevation of about 1330-1350 meters above sea level (masl). The Pearsons Canyon trench site is located at an elevation of about 1380 masl, approximately 1.5 miles south of Willard, Utah. Local vegetation at these sites includes oak (*Quercus*), sagebrush (*Artemisia*), and grasses (Poaceae).

Trenches were excavated at these three sites to investigate Wasatch fault scarps formed on post-Bonneville (~mid-Holocene and younger) alluvial fan deposits. The fan deposits are derived from narrow drainage basins in the Wasatch Range that have maximum elevations of about 2300 meters. Bulk organic matter from the trenches was collected from paleosols developed on alluvial-fan deposits and scarp-derived colluvium, mixed soil organics within scarp-derived colluvium, and mixed soil organics from the matrices of debris flows. Paleosols are noted to have developed on coarse alluvial-fan deposits. These paleosols ranged from about 10 to 30 cm thick and consist mostly of silt- and clay-rich, root-mixed, dark brown A horizons. Evidence for single surface-faulting earthquakes was found at the Hanson Canyon and Pearsons Canyon sites, while evidence for two paleoevents was noted at the Kotter Canyon site. Samples from buried soils, fault-scarp colluvium, and post-faulting debris flows will help constrain the timing of the paleoearthquakes at these sites.

Hansen Canyon

Samples HC-R1 through HC-R6 were taken from the North trench at the Hansen Canyon site. Sample HC-R1 represents buried soil below a colluvial wedge (Table 1). This sample several small fragments of both conifer and hardwood charcoal weighing a total of 0.0015 g (Table 2, Table 3). The sample also contained a moderate amount of uncharred rootlets from modern plants, a few insect eggs, and a few snail shells.

Several small fragments of charcoal weighing a total of 0.0013 g were present in sample HC-R2 from buried soil below a colluvial wedge. These charcoal fragments were too small for further identification. Two uncharred Poaceae caryopses reflect modern grasses at the site. In addition, the sample contained a moderate amount of uncharred rootlets, two insect chitin fragments, a few insect eggs, and snail shells.

Sample HC-R3 from buried soil below a debris flow yielded 13 fragments of charcoal too small for identification and weighing 0.0004 g. A moderate amount of uncharred rootlets reflect modern plants. Non-floral remains include an uncharred bone fragment, a rodent molar (tooth), two insect chitin fragments, and a few snail shells.

Sample HC-R4 from buried soil below a debris flow contained several fragments of charcoal weighing 0.0005 g. These charcoal fragments were too small for further identification. One uncharred *Polygonum* seed fragment, a few uncharred root fragments, and a moderate amount of uncharred rootlets represent modern plants. The sample also yielded a few insect chitin fragments, a rodent tooth enamel fragment, and a snail shell.

Sample HC-R5 was collected from a debris flow. This sample contained several fragments of charcoal too small to identify and weighing 0.0006 g. Recovery of a small earthworm, ten insect chitin fragments, a few insect eggs, two insect puparia fragments, and two rodent tooth fragments suggests subsurface disturbance from earthworm, insect, and rodent activity in the area. One uncharred bone fragments also was recovered. The presence of uncharred *Astragalus*, *Chenopodium*, and *Portulaca* seeds/seed fragments, as well as a moderate amount of uncharred rootlets, also notes introduction of modern material into these sediments.

Seven fragments of charred, PET fruity tissue weighing 0.0005 g were present in sample HC-R6 from a debris flow. The term PET (processed edible tissue) was originated by Nancy Stenholm (1994) and refers to softer tissue types, such as starchy parenchymoid or fruity epitheloid tissues. PET fruity tissues resemble sugar-laden fruit or berry tissue without the seeds, as well as tissue from succulent plant parts such as cactus pads. Several small fragments of charcoal weighing 0.0004 g and too small for identification also were noted. An uncharred *Astragalus* seed and a moderate amount of uncharred rootlets reflect modern plants.

Samples HC-R7 and HC-R8 were recovered from buried soil beneath a colluvial wedge in the South trench at the Hansen Canyon site. Both samples yielded small fragments of charcoal too small for identification weighing 0.0012 g and 0.0006 g, respectively. These samples also yielded a few uncharred rootlets from modern plants and a few uncharred bone fragments. In addition, sample HC-R7 contained a small piece of coal, two insect chitin fragments, a few insect eggs, an insect puparia and puparia fragment, and a few snail shell fragments.

Sample HC-R9 from a debris flow yielded several fragments of charcoal too small for identification and weighing 0.0014 g. A few insect chitin and puparia fragments reflect minimal subsurface disturbance from insect activity in the area. A moderate amount of uncharred rootlets and a few uncharred bone fragments also were noted.

Kotter Canyon

The Kotter Canyon site yielded evidence for two paleoevents. A weak soil developed on the younger of two colluvial-wedge deposits. Dating charcoal in bulk soil samples from buried soils, fault-scarp colluvium, and a post-faulting debris flow should provide timing information for the two events. Samples KC-R2 and KC-R4 represent buried soil on P1 colluvial wedge, buried by a debris flow. Sample KC-R2 contained one fragment of charcoal too small for identification and weighing less than 0.0001 g. One uncharred *Artemisia* seed reflects modern sagebrush in the area. A few insect chitin fragments and a piece of rodent tooth enamel indicate limited bioturbation from insect and rodent activity. A few fragments of charcoal too small for identification and weighing 0.0001 g were present in sample KC-R4. In addition, a few uncharred rootlets from modern plants, an uncharred bone fragment, and a few small fragments of coal were noted.

Fragments of charcoal too small for identification weighing 0.0001 g and 0.0003 g, respectively, were present in samples KC-R3 and KC-R11 from buried soil on an alluvial fan, buried by P2 colluvial wedge. These samples also yielded a few uncharred rootlets from

modern plants, uncharred bone, and a few insect chitin fragments. A few small pieces of coal were recovered in sample KC-R11.

Samples KC-R6 and KC-R7 were taken from the debris flow. Sample KC-R6 contained several fragments of charcoal too small for identification and weighing 0.0007 g. Uncharred *Artemisia*, *Astragalus*, and *Euphorbia* seeds/seed fragments, as well as a moderate amount of rootlets, represent modern plants in the area. Non-floral remains include two uncharred bone fragments, a few pieces of coal, a few insect chitin fragments, an insect puparia, and an ant. The sample also yielded a few sclerotia. Sclerotia are commonly called "carbon balls". They are small, black, solid or hollow spheres that can be smooth or lightly sculpted. These forms range from 0.5 to 4 mm in size. Sclerotia are the resting structures of mycorrhizae fungi, such as *Cenococcum graniforme*, that have a mutualistic relationship with tree roots. Many trees are noted to depend heavily on mycorrhizae and may not be successful without them. "The mycelial strands of these fungi grow into the roots and take some of the sugary compounds produced by the tree during photosynthesis. However, mycorrhizal fungi benefit the tree because they take in minerals from the soil, which are then used by the tree" (Kricher and Morrison 1988:285). Sclerotia appear to be ubiquitous and are found with coniferous and deciduous trees including *Abies* (fir), *Juniperus communis* (common juniper), *Larix* (larch), *Picea* (spruce), *Pinus* (pine), *Pseudotsuga* (Douglas fir), *Alnus* (alder), *Betula* (birch), *Populus* (poplar, cottonwood, aspen), *Quercus* (oak), and *Salix* (willow). These forms originally were identified by Dr. Kristina Vogt, Professor of Ecology in the School of Forestry and Environmental Studies at Yale University (McWeeney 1989:229-230; Trappe 1962).

One charred, vitrified tissue fragment was present in sample KC-R7. Vitrified tissue has a shiny, glassy appearance due to fusion by heat. Vitrified tissue might reflect charcoal or other charred plant tissue too vitrified for identification. Several small pieces of charcoal too small for identification yielded a weight of 0.0015 g. Minimal subsurface disturbance is evidenced by recovery of a few insect chitin fragments, a few insect eggs, and a rodent tooth enamel fragment. Six small uncharred bone fragments also were noted.

Sample KC-R8 was collected from buried soil on the alluvial fan, buried by colluvial wedge in graben. Four fragments of charcoal too small for identification were present in this sample and weighed 0.0007 g. A moderate amount of uncharred rootlets from modern plants and a few insect chitin fragments and eggs also were recovered.

Pearsons Canyon

At the Pearsons Canyon site, samples were recovered from a soil developed on alluvial-fan deposits that had been faulted down to the west by a single paleoearthquake and buried by scarp colluvium. Five samples were collected from the South trench. Sample PCN-R1 represents buried soil beneath a colluvial wedge. This sample contained three fragments of conifer charcoal weighing 0.0002 g and several fragments of charcoal too small for identification weighing 0.0017 g. The sample also yielded a few pieces of coal and a few uncharred rootlets from modern plants.

Sample PC-R2 was taken from the colluvial wedge and contained five fragments of conifer charcoal weighing 0.0009 g, as well as several small, unidentified charcoal fragments

weighing 0.0020 g. An uncharred *Astragalus* seed, a few uncharred root fragments, and a moderate amount of uncharred rootlets reflect modern plants in the area. Non-floral remains include a few coal fragments and a few insect chitin fragments.

One charred *Juniperus* seed fragment weighing 0.0013 g was present in sample PCN-R3 from buried soil beneath the colluvial wedge. This seed fragment is ideal for AMS radiocarbon dating. Five fragments of conifer charcoal weighing 0.0007 g might also represent juniper wood that burned. In addition, the sample contained a few uncharred rootlets from modern plants and a few coal fragments.

Sample PCN-R4 from buried soil beneath the colluvial wedge yielded fragments of conifer charcoal weighing 0.0036 g. A moderate amount of uncharred rootlets and rock/gravel were the only other remains to be recovered.

Sample PCN-R5 represents buried soil below the colluvial wedge near an antithetic fault zone. One charred Poaceae caryopsis fragment reflects local grasses that burned. Several fragments of charcoal too small for identification yielded a weight of 0.0009 g.

Four samples were recovered from the North trench. Sample PCN-R6 was collected from the colluvial wedge. Two charred Poaceae caryopsis fragments weighing less than 0.0001 g and several charred probable Poaceae stem fragments weighing 0.0006 g appear to represent grasses in the area that burned. The charcoal record includes one burned, slightly vitrified unidentified twig fragment weighing 0.0023 g and several pieces of charcoal too small for identification weighing 0.0010 g. The sample also yielded a few insect chitin fragments, a few insect eggs, and a few uncharred rootlets.

Sample PCN-R7 was collected from a debris flow overlying the P1 colluvial wedge in the antithetic fault zone. This sample yielded four fragments of conifer charcoal weighing 0.0017 g and several fragments of charcoal too small for identification weighing 0.0005 g. A moderate amount of uncharred rootlets and an abundance of rock/gravel also were noted.

Samples PCN-R8 and PCN-R9 represent buried soil below the colluvial wedge. Both samples contained charred probable Poaceae stem fragments, weighing less than 0.0001 g and 0.0004 g, respectively. A charred Poaceae caryopsis also was noted in sample PCN-R9. Grasses in this area appear to have burned. Charcoal fragments in these samples were too small for identification. Sample PCN-R8 contained 0.0003 g of charcoal, while sample PCN-R9 yielded 0.0012 g of charcoal. A few small fragments of coal, a few insect chitin and puparia fragments, and an uncharred *Silene* seed also were present in sample PCN-R9.

SUMMARY AND CONCLUSIONS

Flotation of sediment samples from three trench sites in the Brigham City segment of the Wasatch Fault zone, Utah, resulted in recovery of charcoal and other charred botanic remains that can be sent for radiocarbon analysis. Several samples contained charcoal or charred botanic remains in sufficient quantities for AMS radiocarbon dating. Conifer charcoal in samples from trenches at Hansen Canyon and Pearsons Canyon, as well as a charred

Juniperus seed fragment in sample PCN-R3, reflect juniper and possibly other conifer trees in the area. Samples from Pearsons Canyon also yielded charred grass seed fragments and charred probable grass stems, reflecting local grasses that burned.

TABLE 1
PROVENIENCE DATA FOR SAMPLES FROM THE BRIGHAM CITY SEGMENT
OF THE WASATCH FAULT, UTAH

Site/ Trench	Sample No.	Notes	Provenience/ Description	Analysis
Hansen/north	HC-R1	Max P1	Buried soil (below colluvial wedge [CW])	Float/Charcoal ID
Hansen/north	HC-R2	Max P1	Buried soil (below CW)	Float/Charcoal ID
Hansen/north	HC-R3	Max P1	Buried soil (below debris flow [DF])	Float/Charcoal ID
Hansen/north	HC-R4	Max P1	Buried soil (below DF)	Float/Charcoal ID
Hansen/north	HC-R5	Min P1	Debris flow	Float/Charcoal ID
Hansen/north	HC-R6	Min P1	Debris flow	Float/Charcoal ID
Hansen/south	HC-R7	Max P1	Buried soil (below CW)	Float/Charcoal ID
Hansen/south	HC-R8	Max P1	Buried soil (below CW)	Float/Charcoal ID
Hansen/south	HC-R9	Min P1	Debris flow	Float/Charcoal ID
Kotter	KC-R2	Min P1	Buried soil (on P1 CW, buried by DF)	Float/Charcoal ID
Kotter	KC-R3	Max P2	Buried soil (on alluvial fan [AF], buried by P2 CW)	Float/Charcoal ID
Kotter	KC-R4	Min P1	Buried soil (on P1 CW, buried by DF)	Float/Charcoal ID
Kotter	KC-R6	MinP1	Debris flow	Float/Charcoal ID
Kotter	KC-R7	Min P1	Debris flow	Float/Charcoal ID
Kotter	KC-R8	Max P2	Buried soil (on AF, buried by CW in graben)	Float/Charcoal ID
Kotter	KC-R11	Max P2	Buried soil (on AF, buried by P2 CW)	Float/Charcoal ID
Pearsons/south	PCN-R1	Max P1	Buried soil (below CW)	Float/Charcoal ID
Pearsons/south	PCN-R2	Min P1	Colluvial wedge	Float/Charcoal ID
Pearsons/south	PCN-R3	Max P1	Buried soil (below CW)	Float/Charcoal ID
Pearsons/south	PCN-R4	Max P1	Buried soil (below CW)	Float/Charcoal ID
Pearsons/south	PCN-R5	Max P1	Buried soil (below CW near antithetic fault zone [AFZ])	Float/Charcoal ID
Pearsons/north	PCN-R6	Min P1	Colluvial wedge	Float/Charcoal ID
Pearsons/north	PCN-R7	Min P1	Debris flow overlying P1 CW in AFZ	Float/Charcoal ID
Pearsons/north	PCN-R8	Max P1	Buried soil (below CW)	Float/Charcoal ID
Pearsons/north	PCN-R9	Max P1	Buried soil (below CW)	Float/Charcoal ID

TABLE 2
MACROFLORAL REMAINS FROM THE BRIGHAM CITY SEGMENT
OF THE WASATCH FAULT, UTAH

Sample No.	Identification	Part	Charred		Uncharred		Weights/ Comments
			W	F	W	F	
HC-R1	Liters Floated						1.50 L
	Light Fraction Weight						4.98 g
	FLORAL REMAINS:						
	Rootlets					X	Moderate
	CHARCOAL/WOOD:						
	Unidentified - small	Charcoal		29			0.0015 g
	NON-FLORAL REMAINS:						
	Insect	Egg			X		Few
	Rock/Gravel					X	Moderate
	Snail shell					X	Few
HC-R2	Liters Floated						1.40 L
	Light Fraction Weight						2.69 g
	FLORAL REMAINS:						
	Poaceae	Caryopsis			2		
	Rootlets					X	Moderate
	CHARCOAL/WOOD:						
	Unidentified - small	Charcoal		34			0.0013 g
	NON-FLORAL REMAINS:						
	Insect	Chitin				2	
	Insect	Egg			X		Few
	Rock/Gravel					X	Moderate
	Snail shell				11		0.0062 g
	Snail shell					X	Few
HC-R3	Liters Floated						1.35 L
	Light Fraction Weight						10.09 g
	FLORAL REMAINS:						
	Rootlets					X	Moderate
	CHARCOAL/WOOD:						
	Unidentified - small	Charcoal		13			0.0004 g

TABLE 2 (Continued)

Sample No.	Identification	Part	Charred W	Charred F	Uncharred W	Uncharred F	Weights/ Comments
HC-R3	NON-FLORAL REMAINS:						
	Bone						
	Insect	Chitin				2	
	Rock/Gravel					X	Moderate
	Rodent tooth - molar				1		
	Snail shell				1	X	Few
HC-R4	Liters Floated						1.50 L
	Light Fraction Weight						7.37 g
	FLORAL REMAINS:						
	Polygonum	Seed				1	
	Roots					X	Few
	Rootlets					X	Moderate
	CHARCOAL/WOOD:						
	Unidentified - small	Charcoal		16			0.0005 g
	NON-FLORAL REMAINS:						
	Insect	Chitin				X	Few
	Rock/Gravel					X	Moderate
	Rodent tooth enamel					1	
	Snail shell				1		
HC-R5	Liters Floated						1.70 L
	Light Fraction Weight						3.25 g
	FLORAL REMAINS:						
	Astragalus	Seed			1		
	Chenopodium	Seed				1	
	Portulaca	Seed			1		
	Rootlets					X	Moderate
	CHARCOAL/WOOD:						
	Unidentified - small	Charcoal		26			0.0006 g
	NON-FLORAL REMAINS:						
	Bone					1	
	Earthworm				1		
	Insect	Chitin				10	
	Insect	Egg			X		
	Insect	Puparia				2	
	Rock/Gravel					X	Moderate
	Rodent tooth					2	

TABLE 2 (Continued)

Sample No.	Identification	Part	Charred W	Charred F	Uncharred W	Uncharred F	Weights/ Comments
HC-R6	Liters Floated						1.40 L
	Light Fraction Weight						9.16 g
	FLORAL REMAINS:						
	PET Fruity	Tissue		7			0.0005 g
	Astragalus	Seed			1		
	Rootlets					X	Moderate
	CHARCOAL/WOOD:						
	Unidentified - small	Charcoal		13			0.0004 g
	NON-FLORAL REMAINS:						
	Rock/Gravel					X	Moderate
HC-R7	Liters Floated						1.35 L
	Light Fraction Weight						1.89 g
	FLORAL REMAINS:						
	Rootlets					X	Few
	CHARCOAL/WOOD:						
	Unidentified - small	Charcoal		36			0.0012 g
	NON-FLORAL REMAINS:						
	Bone				1	10	Small
	Coal					1	
	Insect	Chitin				2	
	Insect	Egg			X		
	Insect	Puparia			1	1	
	Rock/Gravel					X	Moderate
	Snail shell					X	Few
HC-R8	Liters Floated						1.30 L
	Light Fraction Weight						4.70 g
	FLORAL REMAINS:						
	Rootlets					X	Few
	CHARCOAL/WOOD:						
	Unidentified - small	Charcoal		19			0.0006 g
	NON-FLORAL REMAINS:						
	Bone					5	
	Rock/Gravel					X	Moderate

TABLE 2 (Continued)

Sample No.	Identification	Part	Charred W	Charred F	Uncharred W	Uncharred F	Weights/ Comments
HC-R9	Liters Floated						1.45 L
	Light Fraction Weight						1.54 g
	FLORAL REMAINS:						
	Rootlets					X	Moderate
	CHARCOAL/WOOD:						
	Unidentified - small	Charcoal		23			0.0014 g
	NON-FLORAL REMAINS:						
	Bone					8	
	Insect	Chitin				5	
	Insect	Puparia				2	
	Rock/Gravel					X	Moderate
KC-R2	Liters Floated						1.25 L
	Light Fraction Weight						9.13 g
	FLORAL REMAINS:						
	Artemisia	Seed			1		
	Rootlets					X	Moderate
	CHARCOAL/WOOD:						
	Unidentified - small	Charcoal		1			< 0.0001 g
	NON-FLORAL REMAINS:						
	Insect	Chitin				7	
	Rock/Gravel					X	Moderate
	Rodent tooth enamel					1	
KC-R3	Liters Floated						1.60 L
	Light Fraction Weight						3.03 g
	FLORAL REMAINS:						
	Rootlets					X	Few
	CHARCOAL/WOOD:						
	Unidentified - small	Charcoal		7			0.0001 g
	NON-FLORAL REMAINS:						
	Bone				1		Small
	Insect	Chitin				15	
	Rock/Gravel					X	Moderate

TABLE 2 (Continued)

Sample No.	Identification	Part	Charred		Uncharred		Weights/ Comments
			W	F	W	F	
KC-R4	Liters Floated						0.8 L
	Light Fraction Weight						4.83 g
	FLORAL REMAINS:						
	Rootlets					X	
	CHARCOAL/WOOD:						
	Unidentified - small	Charcoal		9			0.0001 g
	NON-FLORAL REMAINS:						
	Bone					1	
	Coal					X	Few
	Rock/Gravel					X	Moderate
KC-R6	Liters Floated						1.40 L
	Light Fraction Weight						11.51 g
	FLORAL REMAINS:						
	Artemisia	Seed				1	
	Astragalus	Seed			1		
	Euphorbia	Seed			1	1	
	Rootlets					X	Moderate
	Sclerotia				X	X	Few
	CHARCOAL/WOOD:						
	Unidentified - small	Charcoal		39			0.0007 g
	NON-FLORAL REMAINS:						
	Bone					2	
	Coal					X	Few
	Insect	Chitin				11	
	Insect	Puparia			1		
	Ant				1	X	Few
	Rock/Gravel					X	Moderate
KC-R7	Liters Floated						1.40 L
	Light Fraction Weight						5.26 g
	FLORAL REMAINS:						
	Vitrified tissue			1			0.0024 g
	Rootlets					X	Few
	CHARCOAL/WOOD:						
	Unidentified - small	Charcoal		46			0.0015 g

TABLE 2 (Continued)

Sample No.	Identification	Part	Charred		Uncharred		Weights/ Comments
			W	F	W	F	
KC-R7	NON-FLORAL REMAINS:						
	Bone					6	
	Insect	Chitin				8	
	Insect	Egg			X		Few
	Rock/Gravel					X	Moderate
	Rodent tooth enamel					1	
KC-R8	Liters Floated						1.00 L
	Light Fraction Weight						5.66 g
	FLORAL REMAINS:						
	Vitrified tissue			1			0.0001 g
	Rootlets					X	Moderate
	CHARCOAL/WOOD:						
	Unidentified - small	Charcoal		4			0.0007 g
	NON-FLORAL REMAINS:						
	Insect						
	Insect	Egg			X		Few
	Rock/Gravel					X	
KC-R11	Liters Floated						1.20 L
	Light Fraction Weight						4.15 g
	FLORAL REMAINS:						
	Rootlets					X	Few
	CHARCOAL/WOOD:						
	Unidentified - small	Charcoal		11			0.0003 g
	NON-FLORAL REMAINS:						
	Bone					5	
	Coal					X	Few
	Insect	Chitin				2	
	Rock/Gravel					X	Moderate
PCN-R1	Liters Floated						.90 L
	Light Fraction Weight						0.81 g
	FLORAL REMAINS:						
	Rootlets					X	Few
	CHARCOAL/WOOD:						
	Conifer	Charcoal		3			0.0002 g
	Unidentified - small	Charcoal		60			0.0017 g

TABLE 2 (Continued)

Sample No.	Identification	Part	Charred W	Charred F	Uncharred W	Uncharred F	Weights/ Comments
PCN-R1	NON-FLORAL REMAINS:						
	Coal					X	Few
	Rock/Gravel					X	Moderate
PCN-R2	Liters Floated						1.40 L
	Light Fraction Weight						1.84 g
	FLORAL REMAINS:						
	Astragalus	Seed			1		
	Roots					X	Few
	Rootlets					X	Moderate
	CHARCOAL/WOOD:						
	Conifer	Charcoal		5			0.0009 g
	Unidentified - small	Charcoal		50			0.0020 g
	NON-FLORAL REMAINS:						
	Coal					X	Few
	Insect	Chitin				X	Few
	Rock/Gravel					X	Moderate
PCN-R3	Liters Floated						1.00 L
	Light Fraction Weight						1.07 g
	FLORAL REMAINS:						
	Juniperus	Seed		1			0.0013 g
	Rootlets					X	Few
	CHARCOAL/WOOD:						
	Conifer	Charcoal		5			0.0007 g
	NON-FLORAL REMAINS:						
	Coal					X	Few
	Rock/Gravel					X	Moderate
PCN-R4	Liters Floated						1.45 L
	Light Fraction Weight						3.12 g
	FLORAL REMAINS:						
	Rootlets					X	Moderate
	CHARCOAL/WOOD:						
	Conifer	Charcoal		13			0.0036 g
	NON-FLORAL REMAINS:						
	Rock/Gravel					X	Moderate

TABLE 2 (Continued)

Sample No.	Identification	Part	Charred		Uncharred		Weights/ Comments
			W	F	W	F	
PCN-R5	Liters Floated						1.00 L
	Light Fraction Weight						4.67 g
	FLORAL REMAINS:						
	Poaceae	Caryopsis		1			
	Sporobolus	Caryopsis			2		
	Rootlets					X	Moderate
	CHARCOAL/WOOD:						
	Unidentified - small	Charcoal		14			0.0009 g
	NON-FLORAL REMAINS:						
	Insect	Chitin				X	Few
	Rock/Gravel					X	Moderate
PCN-R6	Liters Floated						0.85 L
	Light Fraction Weight						10.01 g
	FLORAL REMAINS:						
	Poaceae	Caryopsis		2			< 0.0001 g
	cf. Poaceae	Stem		26			0.0006 g
	Rootlets					X	Few
	CHARCOAL/WOOD:						
	Unidentified twig - slightly vitrified	Charcoal		1			0.0023 g
	Unidentified - small	Charcoal		19			0.0010 g
	NON-FLORAL REMAINS:						
	Insect	Chitin				X	Few
	Insect	Egg			X		Few
	Rock/Gravel					X	Moderate
PCN-R7	Liters Floated						2.25 L
	Light Fraction Weight						5.21 g
	FLORAL REMAINS:						
	Rootlets					X	Moderate
	CHARCOAL/WOOD:						
	Conifer	Charcoal		4			0.0017 g
	Unidentified - small	Charcoal		11			0.0005 g
	NON-FLORAL REMAINS:						
	Rock/Gravel					X	Numerous

TABLE 2 (Continued)

Sample No.	Identification	Part	Charred		Uncharred		Weights/ Comments
			W	F	W	F	
PCN-R8	Liters Floated						1.50 L
	Light Fraction Weight						16.09 g
	FLORAL REMAINS:						
	cf. Poaceae	Stem		5			< 0.0001 g
	Rootlets					X	Few
	CHARCOAL/WOOD:						
	Unidentified	Charcoal		6			0.0003 g
	NON-FLORAL REMAINS:						
	Rock/Gravel					X	Moderate
PCN-R9	Liters Floated						1.50 L
	Light Fraction Weight						12.48 g
	FLORAL REMAINS:						
	Poaceae	Caryopsis		1			
	cf. Poaceae	Stem		20			0.0004 g
	Silene	Seed			1		
	Rootlets					X	Few
	CHARCOAL/WOOD:						
	Unidentified - small			26			0.0012 g
	NON-FLORAL REMAINS:						
	Coal					X	Few
	Insect	Chitin				13	
	Insect	Puparia				2	
	Rock/Gravel					X	Moderate

W = Whole
F = Fragment
X = Presence noted in sample
L = Liters
g = grams

TABLE 3
INDEX OF MACROFLORAL REMAINS RECOVERED FROM THE BRIGHAM CITY SEGMENT OF THE WASATCH FAULT, UTAH

Scientific Name	Common Name
FLORAL REMAINS:	
Artemisia	Sagebrush
Astragalus	Milkvetch
Chenopodium	Goosefoot, Pigweed
Euphorbia	Spurge
Juniperus	Juniper
Poaceae	Grass family
Polygonum	Smartweed, Knotweed
Portulaca	Purslane
PET fruity tissue	Fruity epitheloid tissues; resemble sugar-laden fruit or berry tissue without the seeds, or succulent plant tissue such as cactus pads
Sclerotia	Resting structures of mycorrhizae fungi
CHARCOAL/WOOD:	
Conifer	Cone-bearing, gymnospermous trees and shrubs, mostly evergreens, including the pine, spruce, fir, juniper, cedar, yew, hemlock, redwood, and cypress
Unidentified - small	Charcoal fragments too small for further identification
Unidentified twig - slightly vitrified	Twig charcoal exhibiting a slightly shiny, glassy appearance due to fusion by heat

REFERENCES CITED

Core, H. A., W. A. Cote and A. C. Day
1976 *Wood Structure and Identification*. Syracuse University Press, Syracuse, New York.

Kricher, John C. and Gordon Morrison
1988 *A Field Guide to Ecology of Eastern Forests*. Houghton Mifflin Company, Boston and New York.

Martin, Alexander C. and William D. Barkley
1961 *Seed Identification Manual*. University of California, Berkeley, California.

Matthews, Meredith H.
1979 Soil Sample Analysis of 5MT2148: Dominguez Ruin, Dolores, Colorado. Appendix B. In *The Dominguez Ruin: A McElmo Phase Pueblo in Southwestern Colorado*, edited by A. D. Reed. Bureau of Land Management Cultural Resource Series. vol. 7. Bureau of Land Management, Denver, Colorado.

McWeeney, Lucinda
1989 What Lies Lurking Below the Soil: Beyond the Archaeobotanical View of Flotation Samples. *North American Archaeologist* 10(3):227-230.

Panshin, A. J. and Carl de Zeeuw
1980 *Textbook of Wood Technology*. McGraw-Hill Book, Co., New York, New York.

Petrides, George A. and Olivia Petrides
1992 *A Field Guide to Western Trees*. The Peterson Field Guide Series. Houghton Mifflin Co., Boston.

Stenholm, Nancy A.
1994 Paleoethnobotanical Analysis of Archaeological Samples Recovered in the Fort Rock Basin. In *Archaeological Researches in the Northern Great Basin: Fort Rock Archaeology since Cressman*, edited by C. M. Aikens and D. L. Jenkins, pp. 531-560. University of Oregon Anthropological Papers 50. Department of Anthropology and State Museum of Anthropology, University of Oregon, Eugene, Oregon.

Trappe, James M.
1962 Fungus Associates of Ectotrophic Mycorrhizae. In *The Botanical Review*. U.S. Department of Agriculture, Washington D.C.

APPENDIX C

SUMMARY OF ^{14}C-DATED CHARCOAL CONCENTRATED FROM BULK SEDIMENT SAMPLES FROM THE HANSEN CANYON, KOTTER CANYON, AND PEARSONS CANYON SITES

SUMMARY OF ^{14}C-DATED CHARCOAL CONCENTRATED FROM BULK SEDIMENT SAMPLES FROM THE HANSEN CANYON, KOTTER CANYON, AND PEARSONS CANYON SITES

Sample	Trench	Location[1] (m)	Material sampled[2]	Unit	Material dated[3] (weight in mg)	Relation to earthquake	Laboratory age[4] (^{14}C yr B.P.)	Mean age ± 2σ[5] (cal yr B.P.)
Hansen Canyon site								
HC-R1	north	16.1, 7.4	Buried soil	3A	29 frag. UC (1.5)	Max HC1	4410 ± 35	**5000 200**
HC-R2	north	16.5, 7.3	Buried soil	3A	34 frag. UC (1.3)	Max HC1	5950 ± 40	**6780 100**
HC-R3	north	18.5, 7.4	Buried soil	3A	13 frag. UC (0.4)	-	sample not dated	**-** **-**
HC-R4	north	19.3, 7.3	Buried soil	3A	16 frag. UC (0.5)	-	sample not dated	**-** **-**
HC-R5	north	16.2, 7.8	Debris flow	1	26 frag. UC (0.6)	Min HC1	2120 ± 35	**2100 140**
HC-R6	north	17.5, 7.6	Debris flow	1	13 frag. UC (0.4)	Min HC1	320 ± 60	**380 160**
HC-R7	south	11.3, 7.2	Buried soil	3A	36 frag. UC (1.2)	Max HC1	3840 ± 35	**4260 140**
HC-R8	south	11.7, 7.2	Buried soil	3A	19 frag. UC (0.6)	Max HC1	4200 ± 25	**4740 120**
HC-R9	south	11.7, 7.5	Debris flow	1	23 frag. UC (1.4)	Min HC1	725 ± 30	**670 60**
Kotter Canyon site								
KC-R2	-	19.6, 12.0	Buried soil	2A	1 frag. UC (<0.1)	-	sample not dated	**-** **-**
KC-R3	-	20.0, 11.4	Buried soil	3A	7 frag. UC (0.1)	Poor max KC2	4590 ± 100	5260 320
KC-R4	-	20.4, 11.7	Buried soil	2A	9 frag. UC (0.1)	Min KC1	2400 ± 120	**2480 320**
KC-R6	-	20.9, 11.9	Debris flow	1	39 frag. UC (0.7)	Min KC1	530 ± 35	**550 80**
KC-R7a	-	22.4, 11.3	Debris flow	1	46 frag. UC (1.5)	Min KC1	340 ± 30	**390 100**
KC-R7b	-	22.4, 11.3	Debris flow	1	1 frag. VT (2.4)	Poor max KC2	4500 ± 30	5170 160
KC-R8	-	25.5, 9.7	Buried soil	3A	4 frag. UC (0.7)	Min KC2/Max KC1	3110 ± 40	**3330 100**
KC-R11	-	20.7, 11.2	Buried soil	3A	11 frag. UC (0.3)	Min KC2/Max KC1	2300 ± 120	**2340 360**
Pearsons Canyon site								
PC-R1	south	11.5, 7.1	Buried soil	3bA	60 frag. UC (1.7)	Poor max PC1	3020 ± 35	3230 120
PC-R2	south	11.7, 7.4	Scarp colluvium	2	50 frag. UC (2.0)	Min PC1	1270 ± 30	**1220 80**
PC-R3	south	12.0, 7.0	Buried soil	3bA	1 Juniperus seed (1.3)	Poor max PC1	4610 ± 25	5380 120
PC-R4	south	13.2, 6.7	Buried soil	3bA	13 frag. conifer (3.6)	Max PC1	1810 ± 30	**1750 100**
PC-R5	south	34.6, 2.9	Buried soil	3dA	14 frag. UC (0.9)	-	320 ± 15	380 80
PC-R6a	north	22.3, 5.4	Scarp colluvium	2	1 twig; UC (2.3)	Min PC1	795 ± 30	**710 40**

PC-R6b	north	22.3, 5.4	Scarp colluvium	2	19 frag. UC (1.0)	Poor min PC1	400	±	35	440	120
PC-R7	south	35.2, 2.9	Debris flow	1	4 frag. conifer (1.7)	Min PC1	1320	±	25	**1250**	**80**
PC-R8	north	22.3, 5.2	Buried soil	3bA	6 frag. UC (0.3)	Max PC1	2100	±	65	**2100**	**200**
PC-R9	north	23.0, 5.1	Buried soil	3bA	26 frag. UC (1.2)	Max PC1	1280	±	30	**1220**	**80**

[1] Location information is horizontal and vertical meter marks on the trench maps (plates 1-3).

[2] Sediment and soil organics sampled for radiocarbon dating. Kotter Canyon samples KC-R1, -R5, and -R9-10 were not sorted for charcoal and are not included here.

[3] Charcoal fragments (and other organic material) sorted from the bulk-soil samples and identified by Paleo Research Institute. UC - unidentified charcoal, VT - vitrified plant tissue.

[4] Laboratory-reported ^{14}C age with one standard-deviation uncertainty. B.P. is before present (1950).

[5] Mean and two-sigma, calendar-calibrated age rounded to nearest decade and determined using OxCal calibration software (v. 4.1; Bronk Ramsey, 1995, 2001) and the IntCal 2009 atmospheric data set (Reimer and others, 2009). Bold text indicates ages included in the OxCal models (appendix E).

APPENDIX D

OPTICALLY STIMULATED LUMINESCENCE AGES FOR THE KOTTER CANYON SITE

OPTICALLY STIMULATED LUMINESCENCE AGES FOR THE KOTTER CANYON SITE

Sample No.[1]	Location (m)[1]	Unit sampled	Material sampled	Water content (%)[2]	K (%)[3]	Th (ppm)[3]	U (ppm)[3]	Cosmic dose additions (Gy/kyr)[4]	Total dose rate (Gy/kyr)	Equivalent dose (Gy)	Aliquots (n)[5]	Laboratory age (±1σ) (yr)[6]
KC-L1	9.4, 8.6	4c	fine sand and silt	5 (32)	1.31 ± 0.14	7.95 ± 0.23	1.79 ± 0.21	0.21 ± 0.02	2.37 ± 0.07	8.52 ± 0.57	25 (30)	3,600 ± 270
KC-L2	27.3, 9.1	4b	fine sand and silt	Sample not dated		-	-	-	-	-	-	-
KC-L3	30.8, 7.3	4c	fine sand and silt	1 (13)	1.15 ± 0.09	5.96 ± 0.21	1.61 ± 0.12	0.22 ± 0.02	2.16 ± 0.06	8.40 ± 0.66	24 (30)	3,900 ± 320

[1] Samples obtained using opaque PVC tubes and analyzed by the U.S. Geological Survey Luminescence Dating Laboratory using quartz blue light. Location information is horizontal and vertical meter marks from the Kotter Canyon trench (plate 2).
[2] Field moisture; complete sample saturation percent in parentheses. Ages calculated using approximately 10% of saturation values.
[3] Analyses obtained using laboratory gamma spectrometry (low-resolution NaI detector).
[4] Cosmic doses and attenuation with depth were calculated using the methods of Prescott and Hutton (1994); Gy – gray.
[5] Number of accepted aliquots; total number of analyses (including failed runs) in parentheses.
[6] Equivalent dose and age for fine-grained 125–250 μm quartz sand; linear plus exponential fit used on age, errors to one standard deviation. Mean age and uncertainty rounded to nearest decade.

APPENDIX E

OXCAL MODELS

OxCal models for the Hansen Canyon, Kotter Canyon, and Pearsons Canyon sites were created using OxCal calibration and analysis software (version 4.1; Bronk Ramsey, 1995, 2001; using the IntCal09 calibration curve of Reimer and others, 2009). The models include *C_Date* for luminescence ages, *R_Date* for radiocarbon ages, and *Boundary* for undated events (paleoearthquakes). These components are arranged into ordered sequences based on the relative stratigraphic positions of the samples. The sequences may contain *phases*, or groups where the relative stratigraphic ordering information for the individual radiocarbon ages is unknown. The models are presented here in reverse stratigraphic order, following the order in which the ages and events are evaluated in OxCal.

Hansen Canyon OxCal Model

```
Plot()
 {
  Sequence("Hansen Canyon 1")
  {
   Boundary("start sequence");
   Phase("Pre HC1 fan soil");
   {
    R_Date("HC-R2", 5950, 40);
    R_Date("HC-R1", 4410, 35);
    R_Date("HC-R8", 4200, 25);
    R_Date("HC-R7", 3840, 35);
   };
   Boundary("HC1");
   R_Date("HC-R5", 2120, 35);
   Phase("young debris flow ages");
   {
    R_Date("HC-R9", 725, 30);
    R_Date("HC-R6", 320, 60);
   };
   Boundary("Sequence end historic constraint", 1847);
  };
 };
```

Kotter Canyon OxCal Model

```
Plot()
```

```
{
 Sequence("Kotter Canyon 3")
 {
  Boundary("Start sequence");
  Phase("Alluvial fan age")
  {
   C_Date("KC-L3", -1900, 320);
   C_Date("KC-L1", -1595, 265);
  };
  Boundary("Earthquake K2");
  Phase("Post-event K2 soil")
  {
   R_Date("KC-R8", 3110, 40);
   R_Date("KC-R11", 2300, 120);
  };
  Boundary("Earthquake K1");
  R_Date("KC-R4", 2400, 120);
  Phase("Unit 1 debris flow")
  {
   R_Date("KC-R6", 530, 30);
   R_Date("KC-R7", 340, 30);
  };
  Boundary("Sequence end historic constraint", 1847);
 };
};
```

Pearsons Canyon OxCal Model

```
Plot()
 {
  Sequence("Pearson Canyon 2")
  {
   Boundary("start sequence");
   Phase("Pre PC1 fan soil")
   {
    R_Date("PCN-R8", 2110, 65);
    R_Date("PCN-R4", 1810, 30);
    R_Date("PCN-R9", 1280, 30);
   };
   Boundary("Earthquake PC1");
   Phase("Post PC1 colluvium")
   {
    R_Date("PCN-R7", 1320, 25);
    R_Date("PCN-R2", 1270, 30);
```

```
  R_Date("PCN-R6a", 795, 30);
  };
  Boundary("Sequence end historic constraint", 1847);
  };
};
```

Hansen Canyon OxCal model 1	Unmodeled (cal yr B.P.)		Modeled (cal yr B.P.)		Agreement
	mean	sigma	mean	sigma	
Sequence					
Boundary start sequence			7880	1140	
Phase Pre HC1 fan soil					
R_Date HC-R2	6780	50	6780	50	100.2
R_Date HC-R1	5000	100	5000	100	99.9
R_Date HC-R8	4740	60	4740	60	99
R_Date HC-R7	4260	70	4260	70	99.1
Boundary HC1			**3140**	**660**	
			HC1 5th-95th: 2100-4220		
R_Date HC-R5	2100	70	2100	70	100.4
Phase young DF ages					
R_Date HC-R9	670	30	670	20	99.2
R_Date HC-R6	380	80	380	70	100.7
Boundary Historic constraint, 1847	100	0	100	0	100

Kotter Canyon OxCal model 3	Unmodeled (cal yr B.P.)		Modeled (cal yr B.P.)		Agreement
	mean	sigma	mean	sigma	
Sequence					
Boundary Start sequence			4140	630	
Phase Mean OSL fan age					
C_Date KC-L3	3850	320	3760	230	111.4
C_Date KC-L1	3550	270	3680	180	109.2
Boundary Earthquake K2			**3520**	**160**	
Phase Post-event K2 soil					
R_Date KC-R8	3330	50	3320	50	97.3
R_Date KC-R11	2340	180	2570	130	69.1
Boundary Earthquake K1			**2450**	**140**	
R_Date KC-R4	2480	160	2320	140	79.7
Phase Unit 1 debris flow					
R_Date KC-R6	550	40	550	40	99.5
R_Date KC-R7	390	50	390	50	99.7
Boundary Historic constraint, 1847	100	0	100	0	100

Pearsons Canyon OxCal model 2	Unmodeled (cal yr B.P.)		Modeled (cal yr B.P.)		Agreement
	mean	sigma	mean	sigma	
Sequence					
Boundary start sequence			2480	450	
Phase Pre PC1 fan soil					
R_Date PCN-R8	2100	100	2080	90	100.6
R_Date PCN-R4	1750	50	1750	50	99.9
R_Date PCN-R9	1220	40	1260	20	94.8
Boundary Earthquake PC1			**1240**	**20**	
Phase Post PC1 colluvium					
R_Date PCN-R7	1250	40	1210	20	59.3
R_Date PCN-R2	1220	40	1190	40	95.3
R_Date PCN-R6a	710	20	710	20	99.7
Boundary Historic constraint, 1847	100	0	100	0	100